

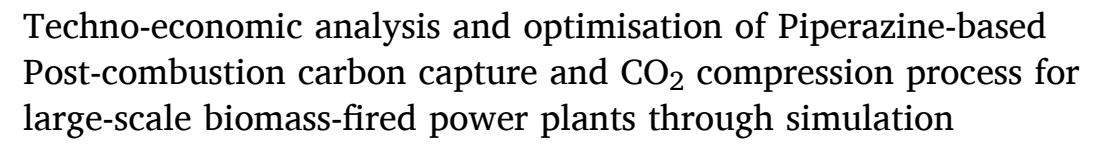
Contents lists available at ScienceDirect

Fuel

journal homepage: www.elsevier.com/locate/fuel



Full Length Article



Jiayi Ren^a, Olajide Otitoju^a, Hongxia Gao^b, Zhiwu Liang^b, Meihong Wang^{a,*}

- ^a Department of Chemical and Biological Engineering, The University of Sheffield, Sheffield S1 3JD, UK
- b College of Chemistry and Chemical Engineering, Joint International Center for CO₂ Capture and Storage (iCCS), Provincial Hunan Key Laboratory for Cost-effective Utilization of Fossil Fuel Aimed at Reducing CO₂ Emissions, Hunan University, Changsha, 410082, PR China

ARTICLE INFO

Keywords: Post-combustion carbon capture Chemical absorption Bioenergy with carbon capture and storage Process simulation Techno-economic analysis Optimisation

ABSTRACT

This study aims to investigate a cost-effective and energy-efficient amine-based post-combustion carbon capture (PCC) process for large-scale supercritical biomass-fired power plants (SC BFPP). Thus, we have quantified the energy and economic performance of the PCC process with different configurations and solvents. Three process configurations which included the standard configuration, the absorber intercooler (AIC) with the advanced flash stripper (AFS) and the AIC, AFS and side stream extraction (SSE) were simulated in Aspen Plus® V11 using 30 wt % and 40 wt% piperazine (PZ) as solvent. In addition to this, CO₂ compression trains using the heat pump (HP) and supercritical CO2 cycle (s-CO2) were also simulated. Sensitivity analysis of the PCC process was carried out to investigate the impact of important parameters on the energy performance of the process. Furthermore, energy analysis shows that a minimum energy consumption of 2.78 GJ/t_{CO2} was achieved with the PCC process using 40 wt% PZ, a combination of the AIC, AFS and SSE for capture and s-CO2 for compression. This achieved a significant energy saving of 1.01 GJ/ $t_{\rm CO2}$ compared with the standard PCC process using 30 wt% monoethanolamine that is used as the benchmark in this study. The economic analysis results showed that the minimum CO2 capture cost of 55.70 \$/t_{CO2} was achieved using the AIC-AFS-SSE-sCO₂ configuration and 40 wt% PZ as solvent. This represents a 19.5 % reduction in cost compared with the standard 40 wt% PZ process with a cost of 69.18 \$/tco2. The optimisation of the PZ-based PCC process was carried out to determine the optimal solvent concentration with the minimum carbon capture cost. It was found that the optimal PZ concentration for the PCC process based on standard and AFS configurations were 37.5 wt% and 32.5 wt%, respectively. The optimisation of the stripper pressure for the minimum carbon capture cost was conducted. As a result, compared with the standard PCC process using 40 wt% PZ, the energy consumption and CO₂ capture cost of the optimised process at the suggested pressure of 7 bar were reduced by 41.6 % and 32.4 %, respectively.

Abbreviations: ACC, Annualized capital cost; AFS, Advanced flash stripper; AIC, Absorber intercooler; APEA, Aspen Process Economic Analyzer; BECCS, Bioenergy with carbon capture and storage; CAPEX, Capital expenditure; CCC, CO2 capture cost; CFPP, Coal-fired power plant; DCC, Direct contact cooler; ELECNRTL, Electrolyte non-random two-liquid; EoS, Equation of state; FGD, Flue gas desulphurization; GHG, Greenhouse gas; GPDC, Generalized pressure drop correlation; HP, Heat pump; IHS, Inter-heated stripper; LHV, Lower heating value; LVC, Lean vapour compression; MEA, Monoethanolamine; MPS, Multi-pressure stripper; MSCC, Multi-stage CO2 compressor; NCCC, National Carbon Capture Centre; NET, Negative emission technology; NGCC, Natural gas combined cycle; O&M, Operating and maintenance cost; OPEX, Operating expenditure; ORC, Organic Rankine cycle; PCC, Post-combustion carbon capture; PFPP, Pulverized fuel power plant; PZ, Piperazine; RK, Redlich-Kwong; RSS, Rich solvent splitting; SC BFPP, Supercritical biomass-fired power plant; s-CO2, Supercritical CO2 cycle; SCR, Selective catalytic reduction; SOC, Stripper overhead compression; SSE, Side stream extraction; TAC, Total annual cost; TSF, Two-stage flash.

E-mail address: Meihong.Wang@sheffield.ac.uk (M. Wang).

^{*} Corresponding author.

Nomenclature

 $c_{p,cw}$ Heat capacity of the cooling water

 $F_{CO_2,OUT} \quad Annual \; CO_2 \; production \; rate$

i Interest rate

 $K_{eq} \qquad \quad Equilibrium \ constants$

n Lifetime

 Q_{cool} Total cooling duty of CO_2 capture and compression

T_{Eva, Sat} Refrigerant saturation temperature

W_{comp} Total compression work

 W_{comp,CO_2} $\,$ Compression work of the standard compression train

 $W_{comp,HP}$ Compression work of the HP compressor

 W_{eq} Total equivalent work W_{heat} Equivalent work of heat duty $W_{net,\,cycle}$ Net power output of the s-CO₂ cycle

W_{pump} Pump work

 φ_{cw} Specific auxiliary power duty

 ΔT_{cw} Temperature increase of the cooling water

1. Introduction

1.1. Background

To mitigate climate change and the global warming caused by the growing CO_2 concentration in the atmosphere, decarbonisation approaches are needed. Energy-related industrial processes are the main source of CO_2 emissions, which reached 36.8 Gt/yr in 2022 [1]. Among the energy-related sectors, power generation is the largest source of CO_2 , accounting for 42 % of global CO_2 emissions [1]. Coal is a vital fuel which has provided over one-third of the global electricity generation [2]. However, coal-fired power plants (CFPPs) would emit a huge amount of CO_2 . It was reported by IEA [2] that the global CO_2 emissions from CFPPs reached 9.7 Gt in 2021. Therefore, to reduce the CO_2 emissions from CFPPs, the following approaches were proposed: (i) to find some substitutes for coal and (ii) to integrate with carbon capture.

Biomass is a clean and renewable energy resource and can be used to co-fire for coal-fired power plants with the minimum changes [3]. More importantly, the growth of biomass materials would consume CO_2 in the atmosphere through photosynthesis, and thus, capturing CO_2 from the combustion or gasification of biomass is a net negative carbon emission process [4]. Therefore, more existing CFPPs are being converted to biomass co-firing or biomass-only pulverized fuel power plants (PFPPs).

The solvent-based PCC is the most mature and commonly applied technology to capture CO_2 from power plants. As the most commonly used benchmark solvent for the amine-based PCC process in most academic studies, monoethanolamine (MEA), would require high energy consumption for regeneration. The energy is provided by the steam extracted from the PFPP, resulting in an efficiency penalty for the power plant. Furthermore, the high capital expenditure (CAPEX) and operating expenditure (OPEX) are also barriers to the commercialization of the PCC process [5].

Currently, the use of new solvents has gained popularity as the solution to improve the energy and economic performance of the PCC process. Piperazine (PZ) a cyclic diamine with a theoretical capacity to capture two moles of CO₂ per mole amine has been proposed as proposed and used. PZ has a higher absorption capacity which would lead to a lower solvent circulation rate and a lower energy requirement for solvent regeneration [6]. Another route to improve energy efficiency is to implement new process configurations. The tests in the pilot plant at the University of Texas presented a new process configuration of advanced flash stripper (AFS) which has been proven to have a better energy performance than the standard configuration [7].

1.2. Literature review

In previous studies, MEA-based PCC was widely applied to power plants such as CFPPs and natural gas combined cycle (NGCC) power plants at a large scale [8–13]. It was presented that the addition of the PCC process would cause a 6 % to 12 % efficiency penalty and a 7 % to 22 % energy penalty to the power plants depending on their types [8,14]. Unlike carbon capture for CFPP and NGCC power plants, fewer studies on large-scale carbon capture for BFPP were found. Ali et al. [12] simulated the standard MEA-based PCC process integrated with an 800 MW SC BFPP. The results showed that applying the CO $_2$ capture and compression process to the BFPP resulted in the plant energy efficiency reduction from 39.3 % to 28.41 %.

The largest proportion of the energy penalty comes from the solvent regeneration process of the PCC [12,15]. MEA as the most used absorbent in the PCC process would require a high heat duty $(3.3–5~{\rm GJ/t}_{\rm CO2})$ for regeneration [16,17]. Thus, to find a solution to the high energy penalty, different process configurations including absorber intercooling, rich solvent splitting (RSS), lean vapour compression (LVC), stripper overhead compression (SOC), multi-pressure stripper (MPS), two-stage flash (TSF) and inter-heated stripper (IHS) were investigated and compared [6,18–20]. Moreover, the energy performance of the PCC process with the combinations of different configurations was also studied [20–23]. The results showed that the combined configurations (e.g. LVC-SOC, MPS-RSS, LVC-RSS-HIS, etc.) can contribute to an energy penalty reduction of 14 % to 37.2 %. However, the positive effect of the improved process configurations on the energy performance of the PCC process is limited by the characteristics of the MEA solvent.

Another approach to reduce the energy consumption of solventbased PCC is to find efficient alternatives to MEA. For solvent-based PCC, the solvents are typically included the amine-based solvents and ionic liquid (IL)-based solvents. The amine-based alternative solvents include the blended, biphasic and non-aqueous amine solvents [24]. What's more, some bio-catalysts (such as Carbonic anhydrase enzyme) were investigated to accelerate the reaction kinetics, enhance the absorption and regeneration process and thus decrease the energy consumption [25]. PZ is also a good alternative to MEA. It shows a better energy performance and a faster reaction rate compared with MEA [26]. Moreover, PZ does not show a significant thermal degradation up to a temperature of 165 °C [27], which allows it to operate under higher reboiler temperatures and higher overhead stripper pressure [28]. Nevertheless, one limitation of PZ is that it would precipitate and generate piperazine hydrate (PZ·6H₂O(s)) at low temperatures under 20 °C and low CO₂ loading [26,29]. What's more, at high CO₂ loading, it would also precipitate and form protonated piperazine carbamate (H+PZCOO-H2O(s)). Thus, to avoid solidification issues, the typical operating temperatures for PCC using 40 wt% PZ are 40 to 150 °C [30]. And the typical range of CO2 loadings is 0.2-0.4 mol CO2/molAlkalinity [31]. Another limitation is that can react with nitrite to form N-nitrosopiperazine (MNPZ), which is a stable nitrosamine and is also known as a type of carcinogen [32].

The experiments of the PCC process using PZ solvent for power plants were carried out in pilot plants. In the separation research program pilot plant at the University of Texas (SRP-UT) at Austin, the tests were carried out using 8 m PZ [6], and different process configurations such as AIC and a two-stage flash stripper were tested. Subsequently, in the pilot-scale tests, a new process configuration named AFS was proposed and tested at the University of Texas and the National Carbon Capture Centre (NCCC) [33,34]. The energy consumption of the PCC process with AFS was 2.1-2.5 GJ/t $_{\rm CO2}$, which is 25 % less compared with the two-stage flash stripper [7].

In addition to the regeneration process, the CO_2 compression process is another source where energy penalty occurs [35]. To retrofit the standard multi-stage CO_2 compression, Muhammad et al. [22] pointed out that using a pump to increase the pressure of the liquefied CO_2 can contribute to pressurization power reduction. Furthermore, Muhammad

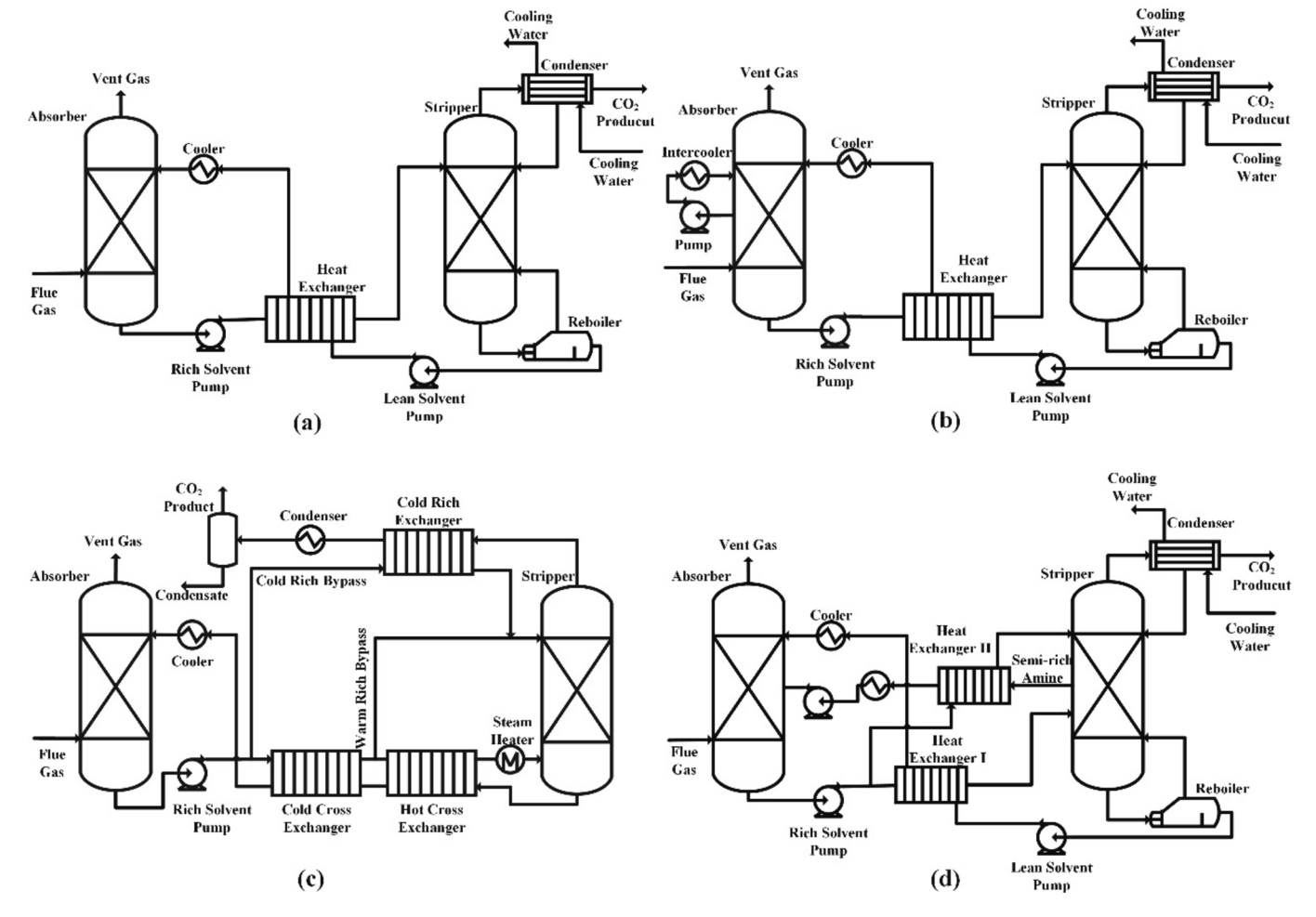


Fig. 1. The flowsheet diagram of solvent-based PCC with different configurations: (a) standard PCC, (b) pump-around AIC, (c)AFS and (d)SSE.

et al. [15] proposed that a heat pump (HP) cycle can be applied to remove the heat of the CO_2 for CO_2 liquefaction.

Moreover, Kurtulus et al. [36] integrated the organic Rankine cycle (ORC) with the compression units, which proposed the feasibility of utilizing the intercooling heat of the compressors for power generation. Subsequently, it was pointed out by Muhammad et al. [22] that the supercritical carbon dioxide (s-CO₂) cycle had a better energy efficiency than ORC theoretically. Hence, the s-CO₂ cycle was applied to the CO₂ compressors to recover the intercooling heat for electricity generation, and to reduce the energy consumption of the compressors.

1.3. Novelty

The specific novelties of this study are as follows:

(1) Simulation of PZ solvent for PCC process for a 550 MW SC BFPP: In previous research, modelling and simulation of solvent-based PCC processes for power plants at large scale were carried out [9–13]. Most of these studies on PCC at a large scale used MEA as the solvent. Several studies on the modelling of large-scale PCC for power plants using PZ were found [35,37–39] and prove it can lower energy consumption compared with MEA. This energy saving was achieved from the advantage of PZ: high CO₂ capacity, and better resistance to oxidative and thermal degradation[26,29,40]. However, all these works focused on PCC for CFPP or NGCC power plants. To the best of this author's knowledge, no studies on modelling and simulation of solvent-based PCC using PZ for BFPPs were conducted. In this work, the model of PZ-based PCC for a 550 MW supercritical BFPP was developed in Aspen Plus® V11.

- (2) Simulation and techno-economic analysis of the PCC process with different process configurations at a large scale: In this work, the model of different process configurations of the PCC process was developed at a large scale, including standard PCC, AIC-AFS and AIC-AFS-SSE. Furthermore, the energy consumption of each configuration and their equivalent work on the BFPP were studied. Also, to evaluate the economic performance of each configuration, their CAPEX and O&M were computed and analysed.
- (3) Simulation and techno-economic analysis of CO₂ compression unit with different process configurations: Otitoju et al. [35] indicated that the CO₂ compression unit is another high-energy-consuming component in addition to the regeneration process in the stripper. A novel configuration of the CO₂ compression process with HP and s-CO₂ cycle was proposed by Muhammad et al. [22]. The results of energy analysis proved that this novel CO₂ compression process can benefit energy performance. However, the economic analysis of applying this new configuration to the PCC process was not carried out. When deploying solvent-based PCC at a large scale, economic performance is one of the most important factors that need to be considered. Therefore, in addition to the energy analysis, a detailed economic analysis was carried out in Aspen Process Economic Analyzer® (APEA) to evaluate the economic performance of the different configurations of the PZ-based PCC.
- (4) Optimisation of CO_2 capture and compression process with different PZ concentrations: The solvent concentration is one of the key parameters that would affect the CO_2 solubility of the solvent and the energy consumption of the regeneration process. Furthermore, no studies have been found on optimizing the economic performance of the

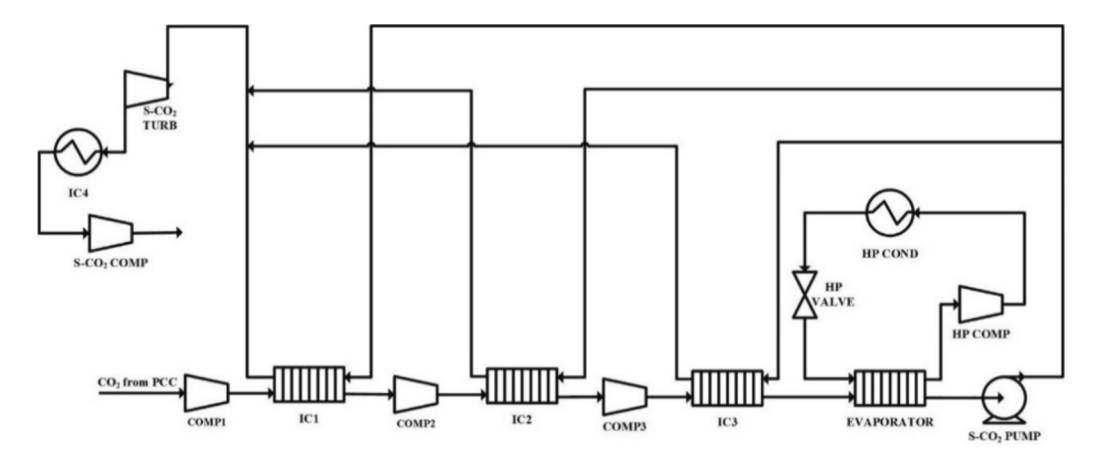


Fig. 2. The flowsheet diagram of the CO₂ compression unit with HP and s-CO₂.

PCC process using PZ with different solvent concentrations. To investigate the effect of the PZ concentration on the $\rm CO_2$ capture cost and find the optimum PZ concentration, process optimisation was carried out for both the standard and the AIC-AFS process configuration.

2. Process description

2.1. Standard PCC process

As shown in Fig. 1(a), the standard PCC process mainly consists of (i) an absorber where the CO_2 in the flue gas is removed by the solvent, (ii) a pump to pressurize the rich solvent, (iii) a heat exchanger to preheat the rich solvent using the hot lean solvent from the stripper, (iv) a stripper where the rich solvent is regenerated under high temperature (usually around 110 $^{\circ}$ C for MEA).

2.2. Pump-around absorber intercooling

Fig. 1(b) presents a typical pump-around absorber intercooling configuration. In the absorber, the lean amine solvent is sprayed from the top stage to absorb the CO_2 in the flue gas and turn to the rich solvent. The intercooler is used in the absorption process to remove a part of the rich solvent from the lower stage, cool it down to 30 °C and send it back to an upper stage. The CO_2 absorption reaction is an exothermic process, so the solvent temperature would rise in the process of reaction. However, it is reported that the optimal reaction temperature is 40–60 °C, and a higher solvent temperature would limit the absorption performance [41]. Therefore, it can reduce the temperature bulge and improve the CO_2 capture level [6].

2.3. Advanced flash stripper

The AFS process configuration is presented in Fig. 1(c). After the CO₂ absorption in the absorber, the rich solvent is pressurized through the pump and split into the cold-rich bypass and a primary flow. The coldrich bypass is heated by the hot overhead vapour from the stripper, while the primary stream is heated in the cold cross exchanger. Then, the outlet-rich solvent from the cold cross exchanger is split into the warm-rich bypass and another primary flow. This primary flow is partially vaporized by a steam heater and is sent to the stripper for the regeneration process. In the stripper, the hot vapour with rich CO₂ is emitted from the top stage, while the lean solvent is cooled through two heat exchangers and a cooler, and circulated to the absorber. In the AFS process configuration, the latent heat of the stripper overhead vapour is utilized to heat the bypass stream [28]. At the same time, the cold-rich bypass is used to cool down the hot outlet vapour from the stripper. Thus, AFS is expected to reduce the heat duty of the PCC process.

Table 1The chemistry of the PCC process using MEA and PZ.

	n dd 1		- HH
No.	Equilibrium reactions (MEA)	No.	Equilibrium reactions (PZ)
1	$2H_2O \mathop{\leftrightarrow} H_3O^+ + OH^-$	1	$2H_2O \leftrightarrow H_3O^+ + OH^-$
2	$CO_2 + 2H_2O \leftrightarrow HCO_3^- +$	2	$CO_2 + 2H_2O \leftrightarrow HCO_3^- + H_3O^+$
	H_3O^+		
3	$HCO_3^- + H_2O \leftrightarrow CO_3^{2-} +$	3	$HCO_3^- + H_2O \leftrightarrow CO_3^{2-} + H_3O^+$
	H_3O^+		
4	$MEAH^+ + H_2O \leftrightarrow MEA +$	4	$PZH^{+} + H_{2}O \leftrightarrow PZ + H_{3}O^{+}$
	H_3O^+		
5	$MEACOO^- + H_2O \leftrightarrow MEA +$	5	$PZ + HCO_3^- \leftrightarrow PZCOO^- + H_2O$
	HCO ₃		
		6	$HPZCOO + H_2O \leftrightarrow PZCOO^- +$
			H_3O^+
		7	PZCOO ⁻ +
			$HCO_3^- \leftrightarrow PZ(COO^-)_2 + H_2O$

2.4. Side stream extraction

Fig. 1(d) shows the amine-based PCC process using side stream extraction (SSE). A part of the semi-rich amine solvent is extracted from the middle stage of the stripper and sent to the middle stage of the absorber. This hot semi-rich amine is used to preheat the bypass of the rich solvent from the absorber.

2.5. CO₂ compression units with HP and s-CO₂

The CO_2 compression units with HP-s CO_2 were developed based on the work of Muhammad et al. [22]. The concentrated CO_2 vapour from the PCC process is sent to the compressors before further utilization or storage. Based on the standard four-stage CO_2 compression units, the compression process is integrated with the heat pump and supercritical CO_2 cycle (shown in Fig. 2). The final stage is replaced by the HP to liquefy the high-pressure CO_2 vapour. Then, the liquefied CO_2 is pressurized by a pump to 200 bar and split into three streams. The split flows are heated by the intercooling heat of the first three stages and mixed. Subsequently, the hot CO_2 fluid is used to drive an s- CO_2 turbine for power generation. The outlet stream from the turbine is cooled down to 30 °C, compressed to 150 bar and transported for storage.

3. Simulation of amine-based PCC process

3.1. Model development of amine-based PCC using MEA and PZ

The rate-based model of the PCC process using MEA and PZ was developed in Aspen Plus® V11. The physical properties of the liquid phase were predicted using the Electrolyte Non-Random Two-Liquid (ELECNRTL) method. The vapour phase was estimated using the

Table 2Kinetic parameters for MEA-based PCC process.

Kinetic reactions	k	E, cal/ mol	Reference
$CO_2 + OH^- \rightarrow HCO_3^-$	4.32e + 13	13,249	Pinsent et al. [47]
$HCO_3^- \rightarrow CO_2 + OH^-$	2.38e + 17	29,451	Aspentech [48]
$\begin{array}{l} \text{MEA} + \text{CO}_2 + \text{H}_2\text{O} \rightarrow \text{MEACOO}^- + \\ \text{H}_3\text{O}^+ \end{array}$	9.77e + 10	9855.8	Hikita et al. [49]
$\begin{array}{l} \text{MEACOO}^- + \text{H}_3\text{O}^+ {\rightarrow} \text{MEA} + \text{CO}_2 + \\ \text{H}_2\text{O} \end{array}$	3.23e + 19	15,655	Hikita et al. [49]

Table 3Kinetic parameters for PZ-based PCC process.

Kinetic reactions	k	E, cal/ mol	Reference
$CO_2 + OH^- \rightarrow HCO_3^-$	4.32e + 13	13,249	Pinsent et al.
$HCO_3^- \rightarrow CO_2 + OH^-$	2.38e + 17	29,451	Aspentech [48]
$PZ + CO_2 + H_2O \rightarrow PZCOO^- + H_3O^+$	4.14e + 10	8038.3	Bishnoi and Rochelle [50,51]
$PZCOO^{-} + H_{3}O^{+} \rightarrow PZ + CO_{2} + H_{2}O$	9.47e + 20	15,333	Aspentech [52]
$PZCOO^{-} + CO_{2} + H_{2}O \rightarrow PZ(COO^{-})_{2} + H_{3}O^{+}$	3.62e + 10	8038.3	Bishnoi and Rochelle [50,51]
$PZ(COO^{-})_{2} + H_{3}O^{+} \rightarrow PZCOO^{-} + CO_{2} + H_{2}O$	3.46e + 20	17,958	Aspentech [52]

Redlich-Kwong (RK) equation of state (EoS). The RK EoS is [42]:

$$p = \frac{RT}{v - b} - \frac{a/T^{0.5}}{v(v + b)} \tag{1}$$

The amine-based CO_2 absorption process contains the equilibrium reactions and the rate-based reactions. The solution chemistry of the MEA and PZ-based CO_2 absorption processes is presented in Table 1.

The temperature-dependent equilibrium constants (K_{eq}) of the equilibrium reactions were calculated using:

$$lnK_{eq} = A + \frac{B}{T} + ClnT + DT$$
 (2)

For the MEA-based PCC process, the coefficients for calculating K_{eq} of reaction (1)-(3) in Table 1 were obtained from Posey & Rochelle [43] while the coefficients of reaction (4) and (5) were obtained from Austgen et al. [44].

For the PZ-based PCC process, the coefficients for calculating $theK_{eq}$ of reaction (1)-(3) were obtained from Posey & Rochelle [43]. The coefficients of reaction (4) were obtained from Hetzer et al. [45], while the coefficients of reaction (5)-(7) were obtained from Ermatchkov et al. [46].

The kinetically controlled reactions were expressed using the power law expression for the reaction rate in Aspen Plus®. The key parameters (pre-exponent factor k and activation energy E) for the kinetically controlled reactions of MEA and PZ-based ${\rm CO_2}$ absorption are presented in Table 2 and Table 3.

For both the MEA and PZ-based models, the density of the liquid mixture was computed using the Rackett model [53], and the gas phase was computed using the RK equation of state [42]. The viscosity of the gas phase was obtained by the Chapman-Enskog-Brokaw model [54], and that of the liquid mixture was obtained by the Jones-Dole electrolyte model [55]. The Wilke-Chang model with Vignes correction [56] was used to calculate the diffusivity of carbon dioxide in the solvent. The Hakim-Steinberg-Stiel model with Onsager-Samaras electrolyte correction [55] was applied to compute the liquid surface tension. The Wassiljewa-Mason-Saxena model [57] and Riedel correction [57] were

Table 4 Operating conditions of the pilot plants.

Solvent	30 wt% MEA	40 wt% PZ
Experimental data	Notz et al.	Plaza and Rochelle [37] for absorber Van Wagener [63] for stripper
Flue gas flow rate (kg/h)	30–100	693.4
Diameter (absorber and stripper) (m)	0.125	0.427
Absorber packing height (m)	4.2	6.1
Stripper packing height (m)	2.52	6.1
Packing type (absorber and stripper)	Mellapak 250Y	Mellapak 2X
CO ₂ in flue gas (wt%)	8.4-16.5	17.6
Lean solvent flow rate (kg/h)	100–300	2916–4608
Lean loading (mol _{CO2} / mol _{amine})	0.096-0.356	0.25-0.33
Absorber pressure (bar)	1.01	1.01
Stripper pressure (bar)	1-2.5	1.38-4.14
Specific reboiler duty (GJ/t _{CO2})	3.68-9.76	3.88-4.59
Capture level (%)	40-88.3	32.0-92.2
CO ₂ mass flow captured (kg/h)	3.4–10.6	39.6–129.6

applied to compute the thermal conductivity of the gas and liquid phases, respectively.

The mass and heat transfer in the absorber and the stripper were predicted using the relevant built-in correlations in Aspen Plus®. For both the absorber and the stripper, the mass transfer coefficients and the interfacial area were predicted by the correlation of Bravo et al. [58]. It is suggested in Stringle [59] that Bravo et al. [58] has a good prediction for the mass transfer characteristics of the structured packings. The heat transfer coefficient was predicted by the Chilton and Colburn method [60]. Additionally, the liquid holdup was predicted by Bravo et al. [61].

3.2. Validation of the amine-based PCC model at pilot scale

The MEA-based PCC process model was validated at a pilot scale using experimental data from Notz et al. [62]. These experimental data were collected based on 30 wt% MEA. The model of the PZ-based PCC process was validated using experimental data from Plaza and Rochelle [37] for the absorber and Van Wagener [63] for the stripper. The inlet parameters and the packing information are presented in Table 4.

Fig. 3 and Fig. 4 present the validation results for the MEA and PZ-based models, respectively. For the MEA-based model, five cases (cases 2, 7, 8, 9 and 29) in Notz et al. [64] with the identical CO_2 partial pressure (109.6 mbar) were selected for validation. While for the PZ-based model, cases 3, 5, 7, 9 and 13 in Plaza and Rochelle [37] and Van Wagener [63] were applied for validation. The parameters of the rich solvent, such as the temperature (Fig. 3(b) and Fig. 4(b)) and the rich loading (Fig. 3 (c) and Fig. 4(c)) were compared with the experimental data. Furthermore, the vital parameters which can reflect the CO_2 absorption performance (CO_2 removal level) were also validated in Fig. 3(a) and Fig. 4(a). Moreover, the specific reboiler duty of the model was also compared with the experimental data and the results are shown in Fig. 3(d) and Fig. 4(d). Consequently, the relative errors were generally within 10 %, which demonstrated that the model can provide a reliable prediction of this PCC process.

3.3. Model scale-up of the amine-based PCC for a 550 MW BFPP

The pilot-scale models were scaled up to process the flue gas from a 550 MW supercritical BFPP reported in NETL [65]. The parameters of the flue gas were taken from Case PN1, the case of 100 % biomass feed. The flue gas consists of CO_2 (15.53 mol%), N_2 (68.37 mol%), O_2 (2.34 mol%), Ar (0.82 mol%) and O_2 (12.94 mol%), The mass flow rate is

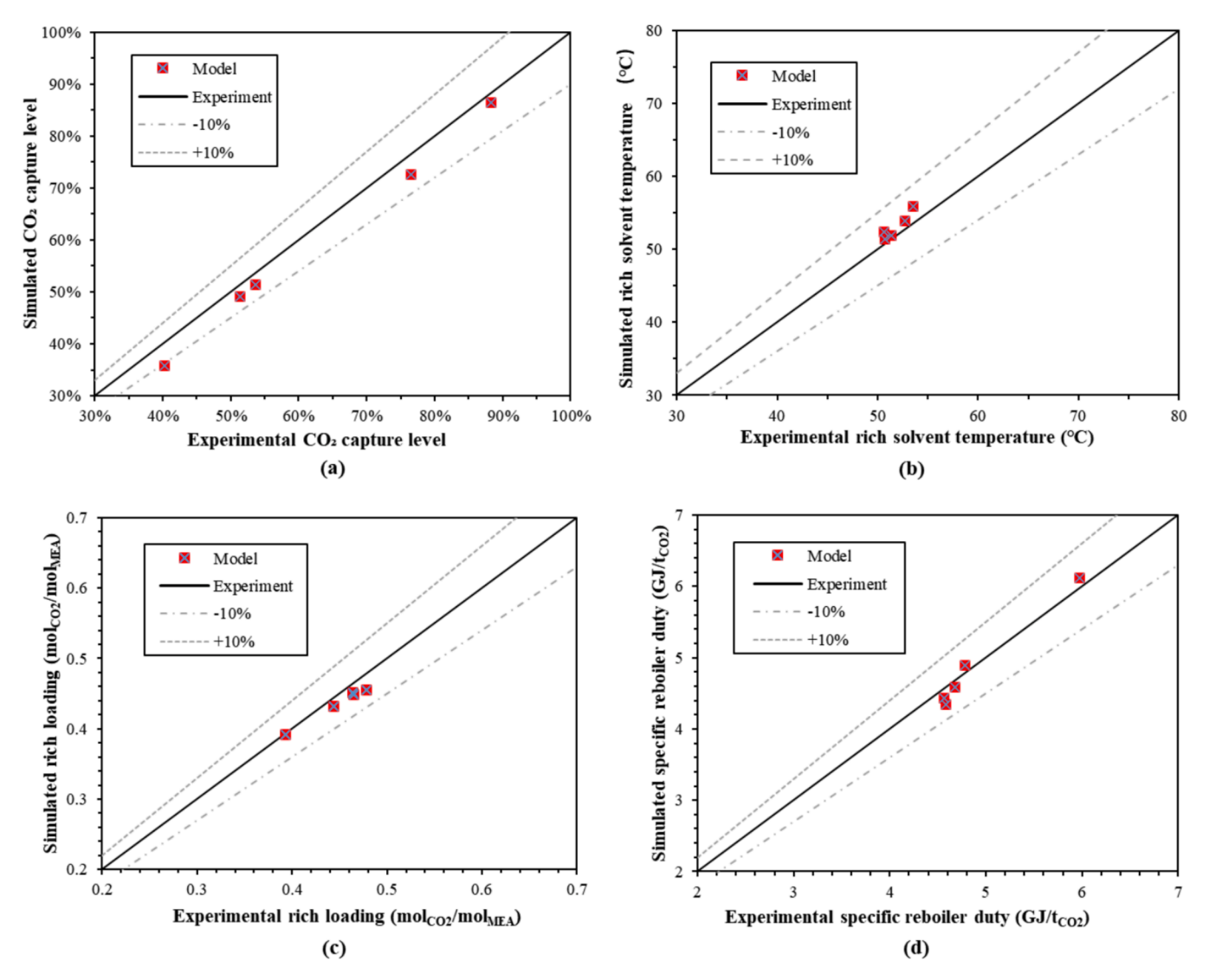


Fig. 3. Experimental data versus model prediction of MEA-based PCC for (a) CO₂ capture level, (b) rich solvent temperature, (c) rich loading and (d) specific reboiler duty.

647.62~kg/s and the inlet temperature is 313.15~K. The capture level was assumed at 90 %. The model was scaled up using the method based on the generalized pressure drop correlation (GPDC) reported by Canepa et al. [8]. The circulation solvent flow rate was estimated based on the method introduced by Agbonghae et al. [66]. The recommended pressure drop per meter packing by Sinnott [67] is around 15–50 mm $\rm H_2O$. In this work, 21 mm $\rm H_2O$ was applied to compute the first-guess design dimensions of the columns. Moreover, the same operating conditions (temperature and pressure) of the absorber and the stripper in the pilot-scale model are used for the large-scale model. It is important to state here that the same packing type (Mellapak 2X) of the absorber and the stripper is used for both the MEA and the PZ cases. This is to eliminate the effect of different packing types on the $\rm CO_2$ absorption performance of the solvents.

The first-guess designs of the large-scale PCC model using 30 wt% MEA and 40 wt% PZ are presented in Table 5. However, it was indicated by Canepa and Wang [68] that the diameter of the columns should be within the structural limit (12.2 m). Thus, more than one absorber is needed. As shown in Fig. 5, the diameter required for using two, three and four absorbers were investigated, which would be 10.4 m, 8.5 m and 7.4 m, respectively. However, the higher number of columns would result in a higher CAPEX without an effective contribution to the $\rm CO_2$ absorption performance. Therefore, in this study, two absorbers each

with a diameter of 10 m were applied. In addition, the stripper diameter of 8 m is within the structural limit (12.2 m), so one stripper was used.

4. Large-scale PCC processes with different configurations

In this section, the performance of different process configurations (AIC-AFS, AIC-AFS-SSE) was investigated. Each type of configuration was simulated using different concentrations (30 wt% and 40 wt%) of PZ as solvent. In addition to the PCC process, different configurations of the $\rm CO_2$ compression units were also studied.

4.1. Simulation of different configurations of the PCC processes

To utilize the heat of the PCC process more efficiently, the AFS process configurations proposed were used (Fig. 6). It was simulated based on the large-scale PZ-based PCC model in Aspen Plus® V11. In the absorber, the pump-around intercooling was simulated using the built-in Pumparounds block configuration subroutine in Aspen Plus®, so it was not shown in the process flowsheet (Fig. 6). This extracts the solvent from the bottom stage, cools it down to 30 °C, and recycles it back to the upper stage. Gao and Rochelle [69] found that pump-around intercooling had a better performance compared with in-out-out intercooling and also could lead to a higher CO₂ capacity. Subsequently, the rich

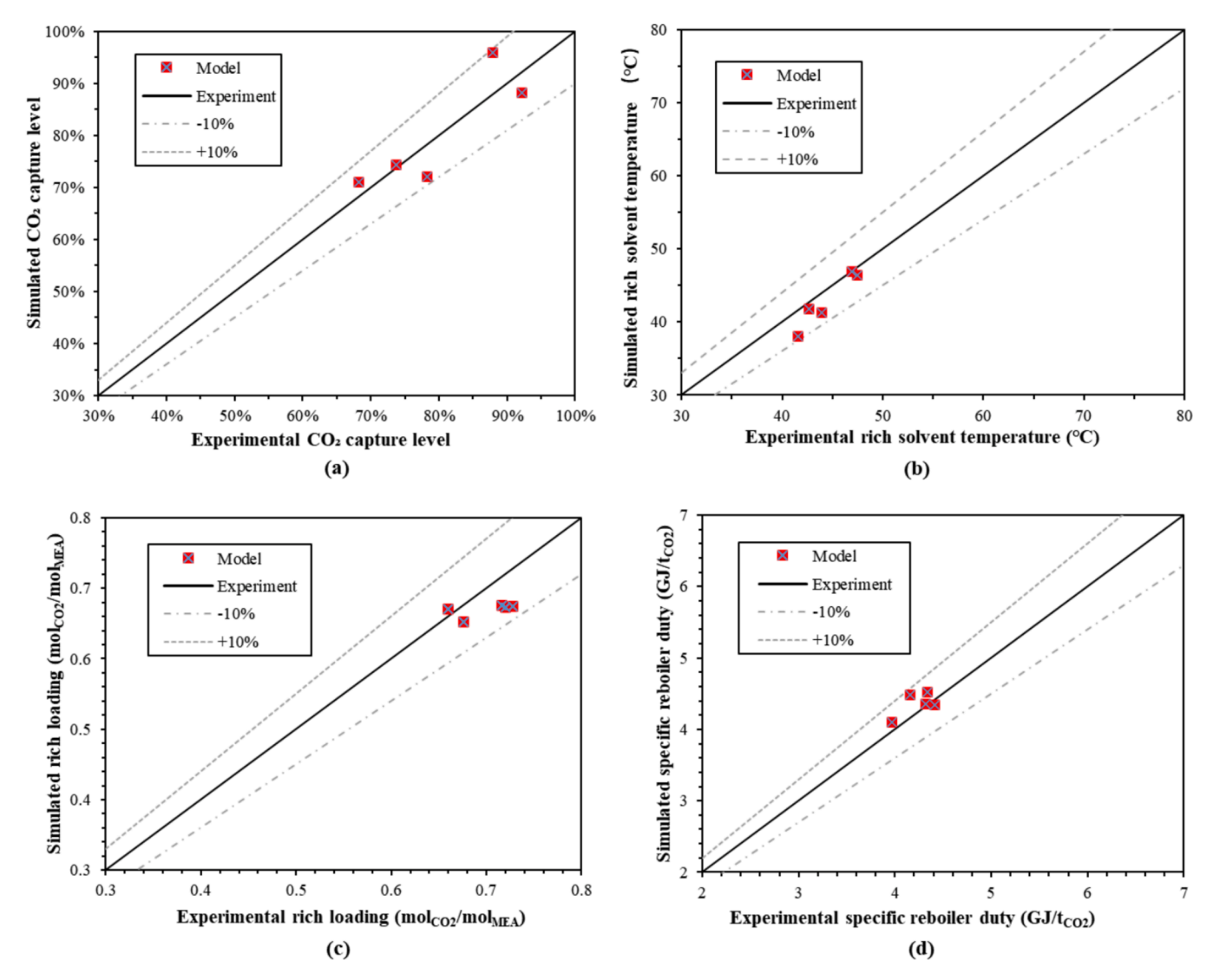


Fig. 4. Experimental data versus model prediction of PZ-based PCC for (a) CO₂ capture level, (b) rich solvent temperature, (c) rich loading and (d) specific reboiler duty.

Table 5The first-guess design dimensions of the standard PCC process at large scale.

Standard PCC process	30 wt% MEA	40 wt% PZ		
Absorber				
Diameter (m)	15	14		
Packing height (m)	25	25		
Packing type	Mellapak 2X	Mellapak 2X		
Flooding capacity	80.80 %	79.05 %		
Stripper				
Diameter (m)	9	8		
Packing height (m)	25	20		
Packing type	Mellapak 2X	Mellapak 2X		
Flooding capacity	79.94 %	73.54 %		

solvent from the absorber was split to the cold and warm rich bypass to recover the latent heat in the stripper overhead vapour. In the AFS configuration, the primary flow was partially vaporised to provide the heat for regeneration in the stripper. The optimum split ratio of the bypasses is investigated in Section 5.3.

As shown in Fig. 7, based on the AFS configuration, a part of the semi-rich solvent is extracted from the middle stage of the stripper to heat the warm-rich bypass and is recycled to the middle of the absorber. Due to less rich solvent being regenerated in the stripper, the required

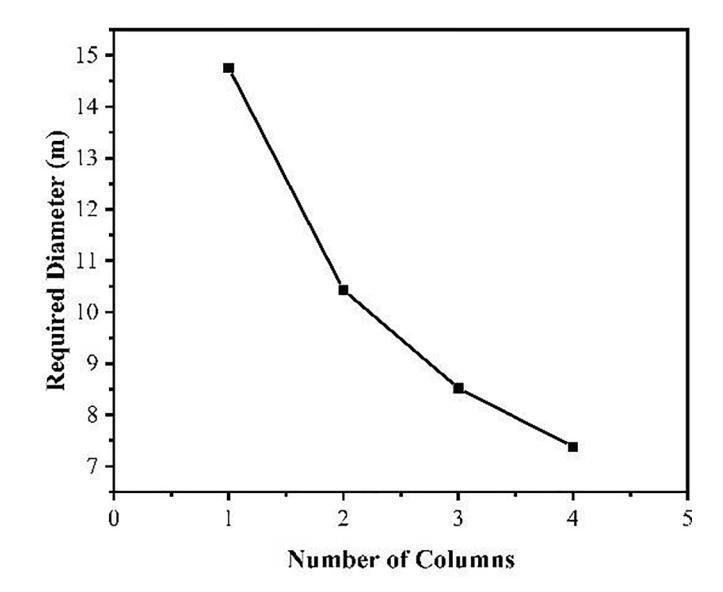


Fig. 5. Required diameter at various numbers of absorber columns (40 wt % PZ).

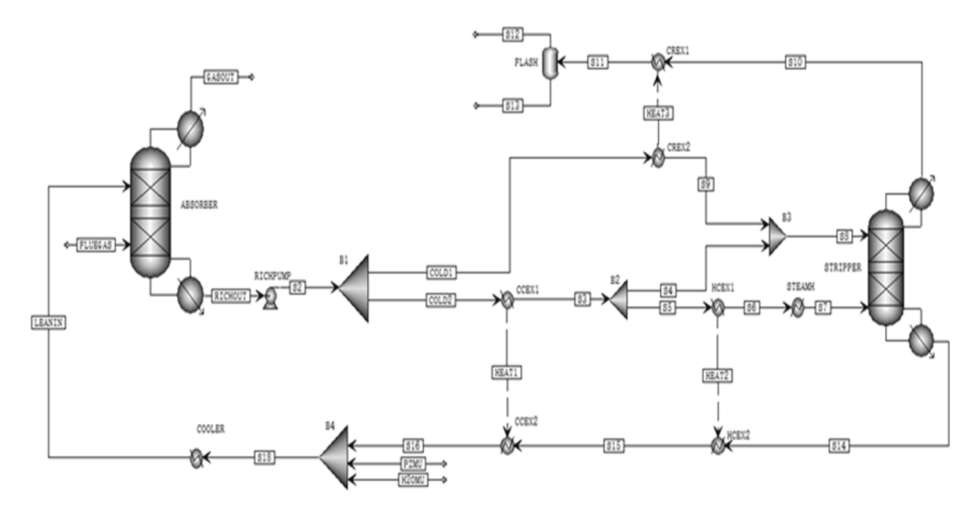


Fig. 6. Process flowsheet of pump-around AIC and AFS.

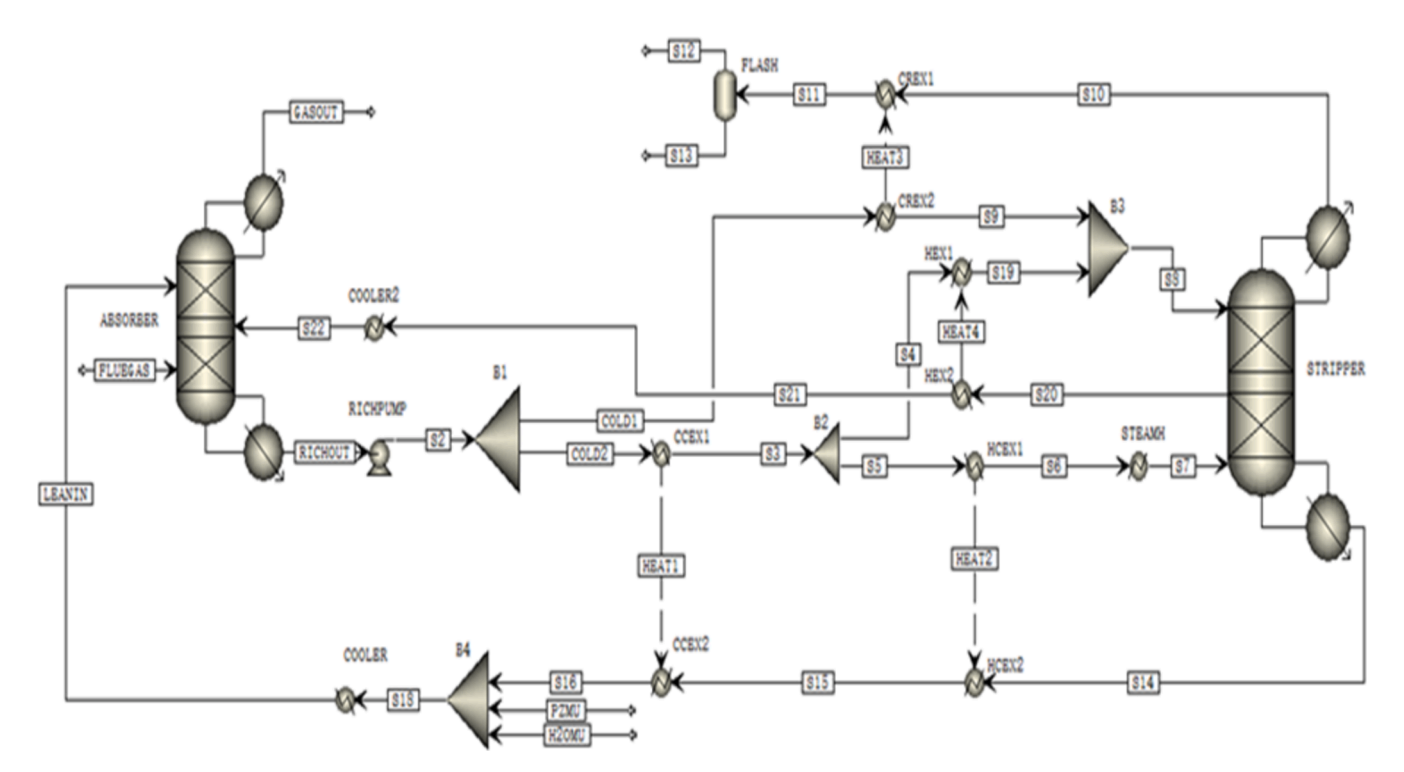


Fig. 7. Process flowsheet of pump-around AIC, AFS and SSE.

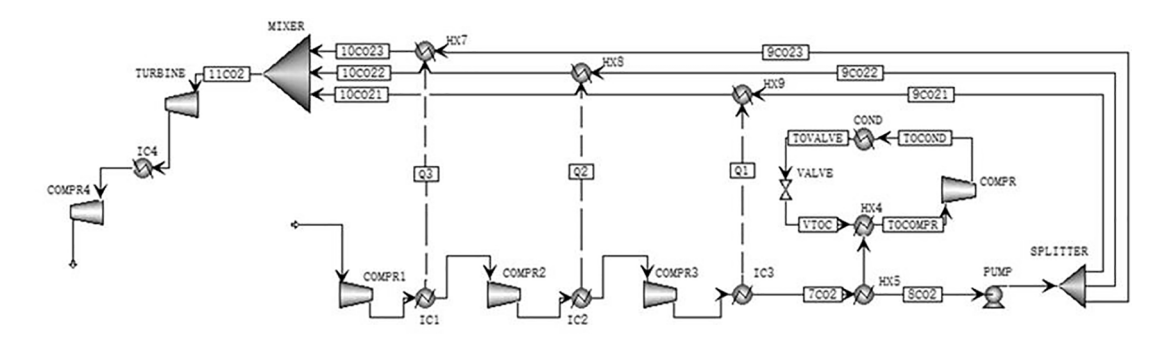


Fig. 8. Process flowsheet of the three-stage CO_2 compression with HP and s- CO_2 cycle.

regeneration energy would be reduced. In addition, the minimum temperature approach of the side-stream heat exchanger is set to 5 $^{\circ}$ C to achieve a higher amount of heat recovery.

4.2. Simulation of different configurations of CO₂ compression processes

In this section, the standard four-stage compressor was simulated to compress the CO_2 from the large-scale PCC plant. Through the compression units, the pressure of the concentrated CO_2 is increased to 150 bar. The intercooler is applied between each stage to cool down the temperature to 30 $^{\circ}$ C.

To reduce the power consumption of the compression units, some modifications are made to the standard four-stage compressor. As shown in Fig. 8, HP is applied to replace the final stage of the standard CO₂ compression train for the liquefaction of the CO₂ using Propane (R290) as the refrigerant. The R290 would remove heat from the compressed CO2, drive the HP cycle and emit the heat to the environment. The pressure of the concentrated CO2 before being liquefied should exceed the triple point pressure of CO₂ (5.18 bar) [70]. Based on the standard CO₂ compression process, the pressure of the CO₂ after the first stage compressor is 10.15 bar. Therefore, the liquefaction process using the HP cycle should be installed after the first stage of the compressor. The CO₂ is liquefied under the saturation temperature at the inlet pressure of the HP cycle. In the evaporator, the pinch point temperature of 5 °C is assumed. And the superheat degree for the refrigerant is assumed to be 5 °C. Subsequently, the HP compressor is assumed as an isentropic compression process with an isentropic efficiency of 80 %. The refrigerant is then cooled down to 30 °C through the HP condenser. Finally, after an isenthalpic expansion process, the refrigerant is recycled to the evaporator.

The liquefied CO_2 is compressed to 200 bar in the pump, split and heated by the intercooling heat from the multi-stage compression process. The outlet temperature of each stage of the compressors can achieve over $100\,^{\circ}\mathrm{C}$. However, in the standard multi-stage compression, the heat of the outlet stream from each compressor is removed using an intercooler, which would also require a certain amount of cooling duty. Therefore, in this s- CO_2 cycle, the intercooling heat is utilized to heat the liquefied CO_2 , while the liquefied CO_2 is also used to cool down the compressor outlet stream. The supercritical CO_2 will work as the working fluid to drive the s- CO_2 turbine for power generation. Subsequently, the outlet CO_2 is cooled and compressed to 150 bar.

5. Sensitivity analysis

To achieve a better energy performance, some important parameters that would possibly affect the CO_2 capture and compression process presented in Section 4.2 were investigated. The effect of lean loading, absorber packing height and stripper pressure on the heat duty of the regeneration process was studied. Moreover, after implementing the AFS configuration, the heat duty at various split ratios was investigated. Subsequently, to figure out the optimal pressure ratio of the s- CO_2 turbine, the relationship between the pressure ratio of the s- CO_2 turbine and the power output of the s- CO_2 cycle was investigated.

5.1. The effect of lean loading on the energy consumption of the regeneration process

The effect of lean loading on the energy performance of the PCC process was investigated based on the model of the standard PCC process integrated with the standard multi-stage $\rm CO_2$ compression (MSCC) unit. The $\rm CO_2$ removal level was kept at 90 % for all the following cases. The energy consumption of different solvents (30 wt% MEA, 30 wt% PZ and 40 wt% PZ) at various lean loading was investigated.

To achieve the low lean solvent loading, more thermal energy will be consumed for the solvent regeneration process. At high values of lean loading, maintaining the CO_2 removal rate at the same level would

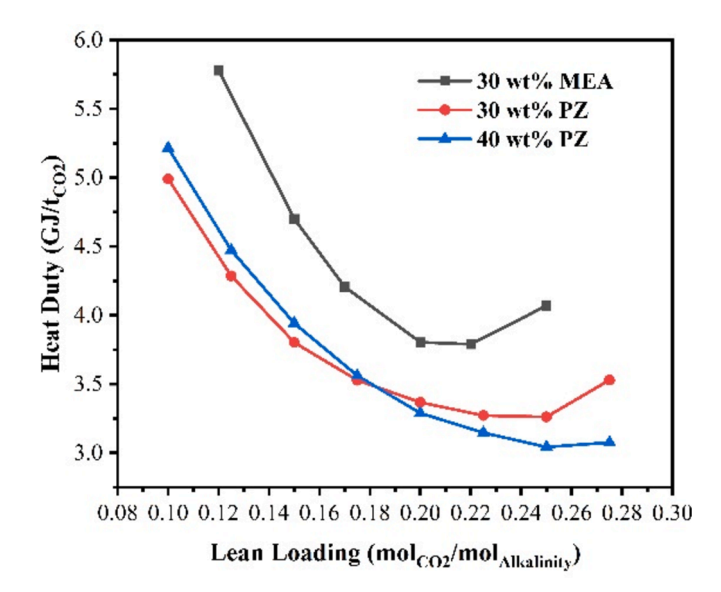


Fig. 9. Energy consumption at various lean loadings for different amines (wt%)

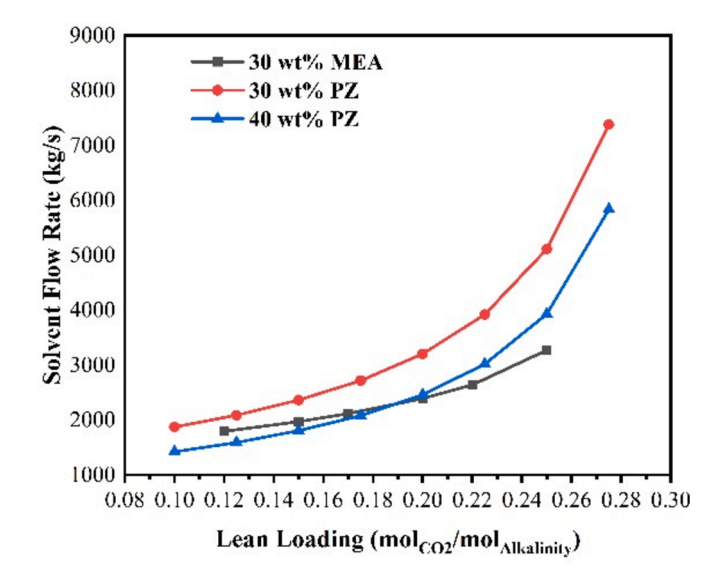


Fig. 10. Solvent flow rate at various lean loading for different amines (wt%).

require a higher solvent flow rate (as shown in Fig. 8). Moreover, to regenerate a higher amount of the rich solvent, more stripping steam will be needed. Therefore, the trade-off between the effect of lean loading and circulation flow rate should be considered together.

In this case, 30 wt% MEA was used as the benchmark. As shown in Fig. 9, at high values of lean loading, the 40 wt% PZ was found to have lower energy consumption than 30 wt% PZ. For the 30 wt% MEA solvent, it achieved the lowest regeneration energy of 3.8 GJ/t_{CO2} at the lean loading of 0.22 mol_{CO2}/mol_{MEA}, which was considered the optimal lean loading for 30 wt% MEA. At the lean loading of 0.25 mol_{CO2}/mol_{Alkalinity}, the minimum heat duty of 30 and 40 wt% PZ of 3.26 and 3.0 GJ/t_{CO2} were achieved, respectively. It showed a 14 %-21 % reduction in heat duty for using PZ compared with the MEA-based case. However, as shown in Fig. 10, at lean loading higher than 0.175 mol_{CO2}/mol_{Alkalinity}, the solvent flow rate had a significant increase with the increasing lean solvent loading. Thus, the lean loading of 0.35 mol_{CO2}/mol_{PZ} was chosen for the cases using 30 wt% and 40 wt% PZ.

What's more, PZ is a diamine, so 1 mol of PZ contains 2 mol of alkalinity. For example, in Fig. 10, the lean loading of 0.10 mol_{CO2} /

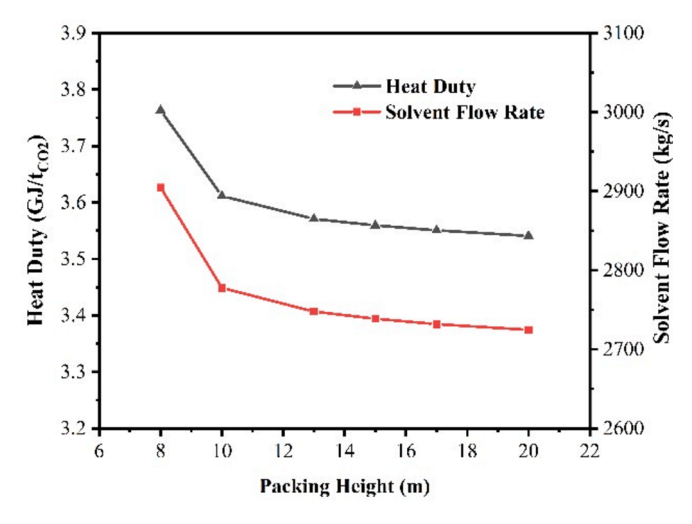


Fig. 11. Heat duty and solvent circulation rate at various absorber packing heights (30 wt% PZ).

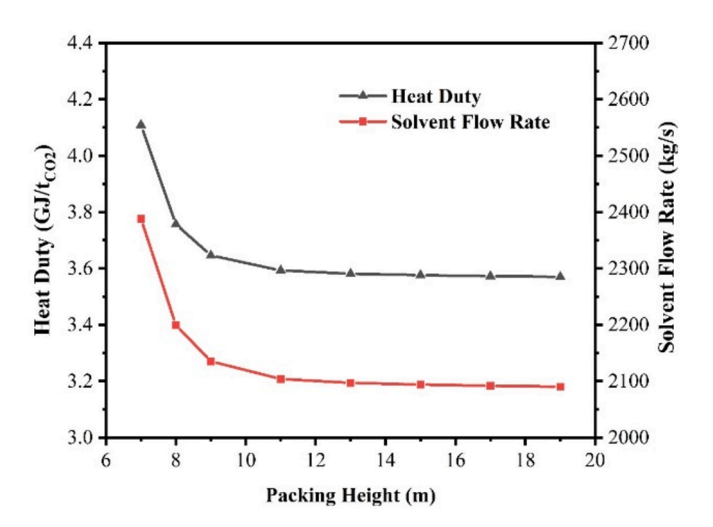


Fig. 12. Heat duty and solvent circulation rate at various absorber packing heights (40 $\,\mathrm{wt}\%$ PZ).

 $\rm mol_{Alkalinity}$ equals 0.20 $\rm mol_{CO2}/\rm mol_{amine}$ for PZ solvent. Therefore, with the lean loading of 0.20 $\rm mol_{CO2}/\rm mol_{amine}$, the solvent flow rate of 30 wt % MEA and PZ were 2389.93 and 1870.45 kg/s, respectively. The results of Fig. 10 also proved that PZ has a higher CO $_2$ capacity than MEA and would require a lower solvent flow rate with the same mass fraction.

5.2. The effect of the absorber packing height on the energy consumption of the PCC process

The effect of absorber packing height on the energy performance of the PCC process was carried out based on the model of the standard PCC integrated with the standard MSCC. The design parameters of Section 3.3 were applied in this case. The same two absorbers with a diameter of 10 m were used. Different absorber packing heights for each absorber varying from 7 m to 19 m were tested. It is shown that the higher absorber packing height would lead to a lower solvent flow rate, which corresponds to a lower regeneration heat requirement. In addition, the lower regeneration heat demand would contribute to the reduction of operating costs. However, at the same time, the larger size of the equipment would lead to the high capital cost of the column. As shown in Fig. 11, for using 30 wt% PZ, significant energy saving was shown with the packing height increase from 8 m to 13 m. At the absorber

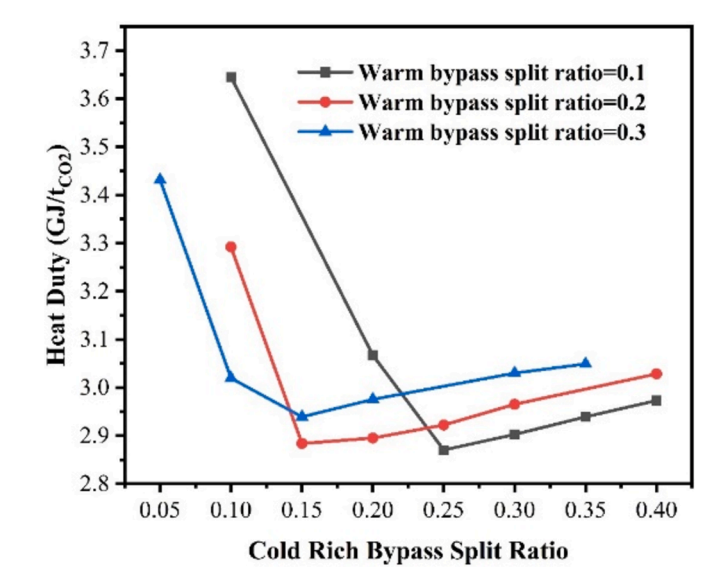


Fig. 13. Heat duty of the PCC process with AFS at various split ratios (30 wt % PZ).

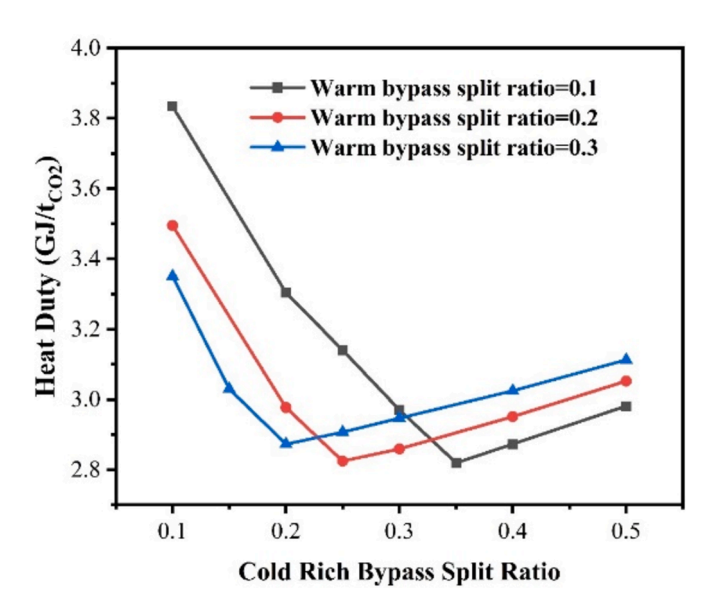


Fig. 14. Heat duty of the PCC process with AFS at various split ratios (40 wt % PZ).

packing height higher than 13 m, the increasing packing height did not show a marked impact on the heat duty reduction. Therefore, in the following cases, 13 m of the absorber packing height was adopted for 30 wt% PZ. For using 40 wt% PZ, a similar trend was found in Fig. 12, so 11 m of the absorber packing height was used.

5.3. The effect of split ratio on the energy performance of the PCC process

The effect of the split ratio on the energy performance of the PCC process was studied based on the model of the PCC process with AIC-AFS integrated with the standard MSCC. In the AFS process configuration, the rich solvent from the rich solvent pump is split twice into the cold rich bypass and the warm rich bypass. To recover the waste heat of the hot streams from the stripper efficiently, the effect of the cold-rich bypass and warm-rich bypass split ratio on the energy performance of the AFS configuration was investigated. The higher cold-rich bypass split ratio can increase the heat recovered from the hot stripper overhead vapour through the cold-rich exchanger. However, it would reduce

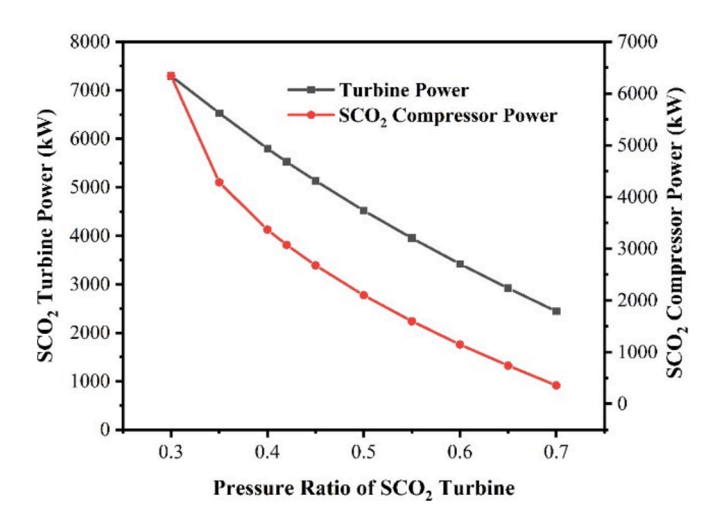


Fig. 15. $S\text{-}CO_2$ turbine power and compressor power at various turbine pressure ratio.

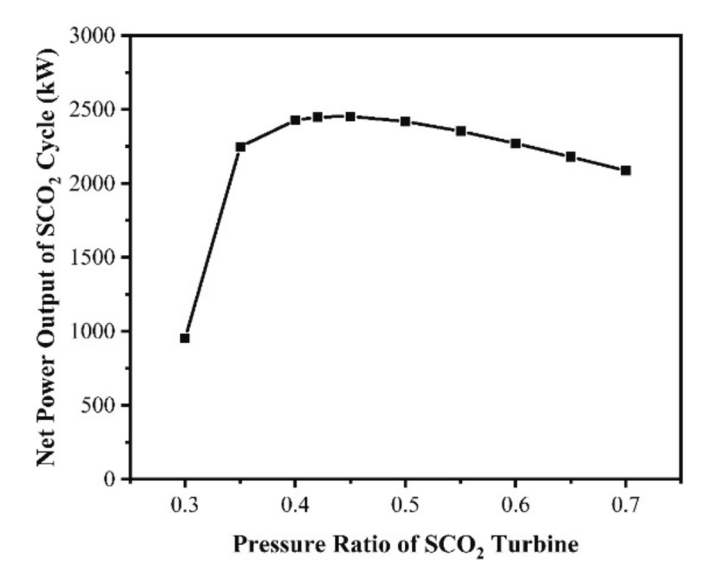


Fig. 16. Net power output of the s-CO₂ cycle at various turbine pressure ratio.

the cold-rich solvent flow rate and the heat recovery in the cold cross exchanger. The warm-rich bypass is used to control the temperature of the stripper inlet flow, which should be around 95–120 $^{\circ}\text{C}$ [71]. Therefore, a higher warm-rich bypass split ratio leads to higher heat recovery in the cold-rich exchanger. Similarly, it would also reduce the heat recovery from the hot outlet lean solvent from the stripper. Consequently, the overall impact is considered and the results are shown in Fig. 13 and Fig. 14 that the optimum cold-rich bypass split ratio for the 30 wt% and 40 wt% cases are 0.25 and 0.35, respectively, with the optimum warm-rich bypass split ratio of 0.1. And the minimum heat duty for the 30 wt% and 40 wt% cases are 2.87 and 2.82 GJ/tco2.

5.4. The effect of the s-CO₂ turbine pressure ratio on the energy consumption of the compression process

The effect of the s-CO $_2$ turbine pressure ratio on the energy performance of the PCC process when using HP-sCO $_2$ was studied. The net power output of the s-CO $_2$ cycle with the s-CO $_2$ turbine pressure ratio varying from 0.3 to 0.7 was investigated. The inlet working fluid pressure of the s-CO $_2$ turbine is controlled at 200 bar. The output pressure of the whole compression unit is fixed at 150 bar.

In the s-CO₂ turbine, the high-pressure ratio represents a high output

pressure and a high-pressure input to the s-CO $_2$ compressor. Therefore, with the fixed inlet and output pressure of the s-CO $_2$ cycle, increasing the pressure ratio of the s-CO $_2$ turbine would reduce the pressure ratio of the s-CO $_2$ compressor. For the s-CO $_2$ turbine, the power output is inversely proportional to its pressure ratio, which is the opposite for the s-CO $_2$ compressor. The results of the s-CO $_2$ turbine power and the s-CO $_2$ compression power with varying s-CO $_2$ turbine pressure ratios are presented in Fig. 15. The sharp decrease of the s-CO $_2$ compressor duty is shown when the pressure ratio of the s-CO $_2$ turbine is between 0.3–0.35. This is because it is close to the critical point, where the density of CO $_2$ changes substantially.

Fig. 16 shows the effect of the s-CO $_2$ turbine pressure ratio on the net power output of the s-CO $_2$ cycle. The net power output of the s-CO $_2$ cycle was calculated as the difference between the s-CO $_2$ turbine power and the s-CO $_2$ compression power. It is shown that the optimal pressure ratio of the s-CO $_2$ turbine in this case is 0.45 generating a net power of 2454.34 kW.

6. Energy analysis

Based on the results of the sensitivity analysis in Section 5, four configurations of the carbon capture and CO_2 compression process with different solvent concentrations (30 and 40 wt% PZ) were simulated. This included standard PCC with standard multistage CO_2 compression, AIC-AFS for PCC integrated with standard multistage CO_2 compression, AIC-AFS-SSE for PCC integrated with standard multistage CO_2 compression and AIC-AFS-SSE for PCC integrated with HP-sCO $_2$ compression unit. The PCC process with standard PCC and standard multistage CO_2 compression using 30 wt% MEA was used as the benchmark case.

The solvent regeneration heat duty is considered as the most important indicator to evaluate the energy performance of the PCC process. The results are summarized in Fig. 17. From the results, using 40 wt% PZ can reduce the heat duty by 0.2 GJ/t_{CO2} compared with the benchmark case. The standard PCC process with 30 and 40 wt% PZ have the same regeneration energy because in Section 5.1 the lean loading of 0.35 mol_{CO2}/mol_{PZ} was chosen for both 30 wt% and 40 wt% PZ cases. From Fig. 9, at this point, they have the same energy consumption of 3.58 GJ/t_{CO2}. Furthermore, compared with the benchmark case, using AIC-AFS configuration can decrease the heat duty by 18.4 % and 21.2 % for 30 and 40 wt% PZ, respectively. Moreover, based on the AFS configuration, extracting a side stream from the stripper can decrease the heat duty by around 0.05 GJ/t_{CO2} for the PZ-based models.

To determine the energy penalty caused by the addition of the PCC to the power plant, the total equivalent work (W_{eq}) of different configurations was evaluated. As shown in Eq. (3), W_{eq} was calculated as the sum of the heat duty work, pumping work and compression work [72].

$$W_{eq} = W_{heat} + W_{pump} + W_{comp} \tag{3}$$

 W_{heat} refers to the equivalent work of heat duty due to the steam extraction from the power plant, and it was obtained using Eq. (4):

$$W_{heat} = \eta_{Turb} \left(\frac{T_{steam} - T_{sink}}{T_{steam}} \right) Q_{reb} \tag{4}$$

where the turbine efficiency (η_{Turb}) is assumed at 90 % [72]. The sink temperature is assumed to be 313 K. The steam temperature is assumed to be the reboiler temperature plus a steam side temperature approach of 10 K. Q_{reb} is the reboiler duty.

In Eq. (3), W_{pump} is the total pump work applied in the PCC process. In the PCC process, pumping power is required to raise the pressure of the rich solvent from the absorber to the required pressure in the stripper. Moreover, the pumping power used to increase the pressure of the liquefied CO_2 should also be considered when applying the compression units with the s- CO_2 cycle. The pumping power is assumed to be provided by the electricity from the power plant. The value of the

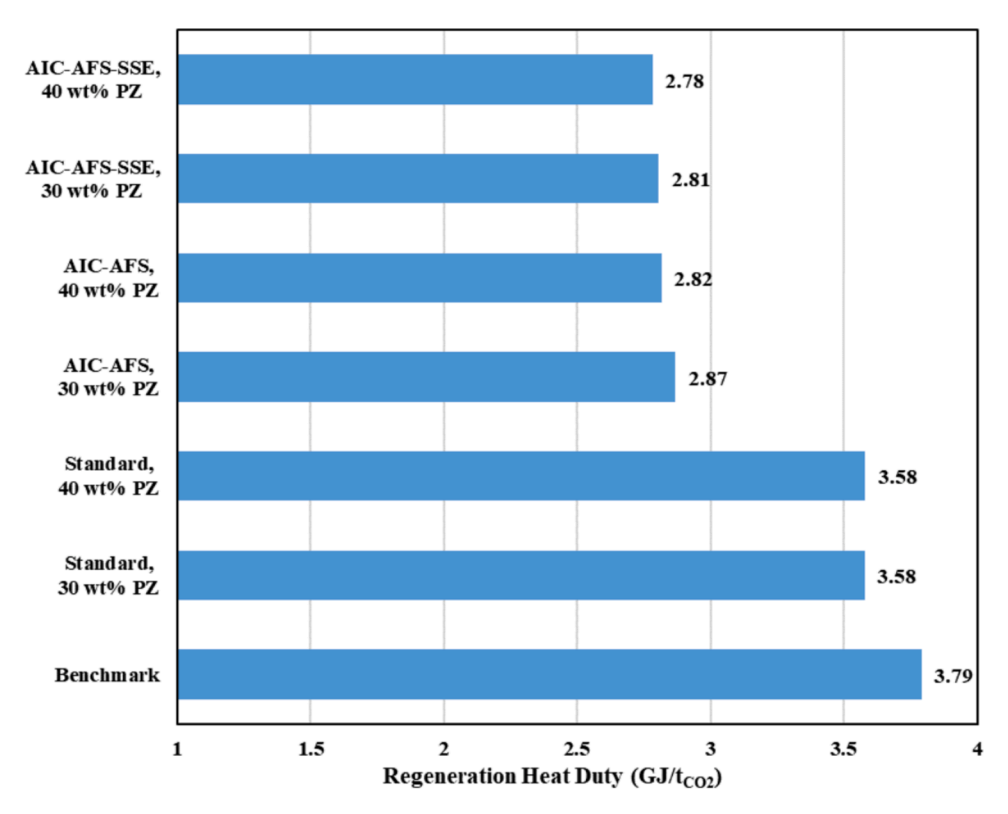


Fig. 17. Regeneration heat duty of different configurations of PCC processes.

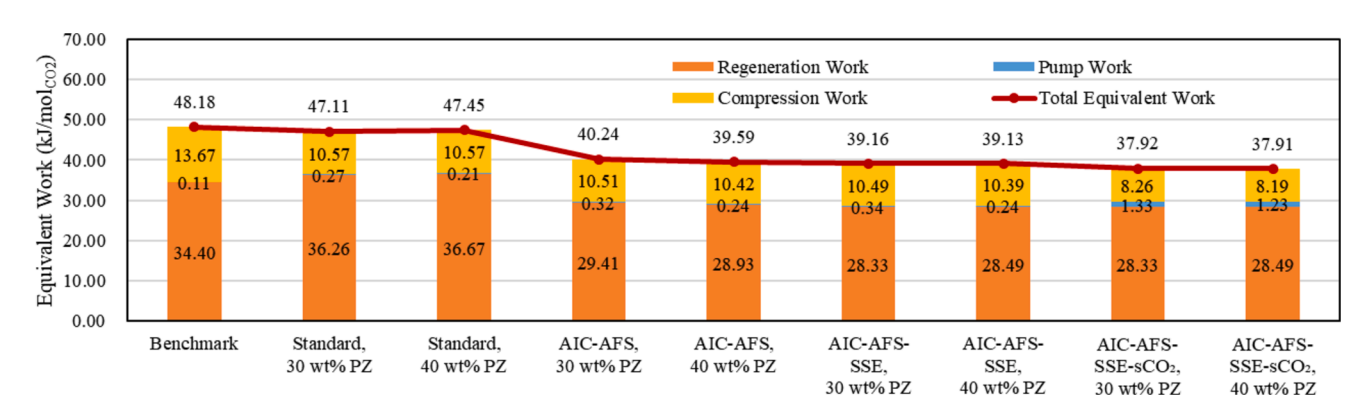


Fig. 18. Distribution of the equivalent work of the different configurations.

pumping power was obtained from the simulation results.

 W_{comp} is the compression work of the compression unit. For the standard CO_2 compression process, the compression work is the sum of the compression duty of each compressor. For the compression units with HP and s- CO_2 , the compression work was calculated using Eq. (5).

$$W_{comp} = W_{comp,CO_2} + W_{comp,HP} - W_{net,cycle}$$
 (5)

where W_{comp,CO_2} is the total compression work of the multi-stage compression train before the CO_2 is liquefied. $W_{comp,HP}$ is the compression work of the compressor in the HP cycle. $W_{net,cycle}$ is the net power output of the s- CO_2 cycle. It was calculated as the difference between the power output of the s- CO_2 turbine and the compression duty of the final-stage compressor.

The calculated equivalent work of solvent regeneration, pumping power and $\rm CO_2$ compression units are presented in Fig. 18. The MEA-based PCC process with the standard configuration was applied as the benchmark. From the results, the regeneration process is the most energy-consuming component in the carbon capture and $\rm CO_2$

compression process. Through using concentrated PZ as the solvent without any improvement on the configuration, the energy saving of around 1 kJ /mol $_{\rm CO2}$ for 30 wt% PZ cases was achieved compared with the benchmark case. Although the standard PCC using 30 and 40 wt% PZ have a lower heat duty than 30 wt% MEA (shown in Fig. 17), the PZ cases have a higher W_{heat} as shown in Fig. 18. This is because the cases of 30 and 40 wt% PZ use a higher stripper pressure of 4.14 bar than the 30 wt% MEA case (1.9 bar). The high stripper pressure would lead to a high reboiler temperature. Thus, based on Eq. (15), the W_{heat} of the PZ cases would be higher than the MEA cases. What's more, the higher stripper pressure, which corresponds to the higher inlet pressure of the $\rm CO_2$ compression unit, is the reason for the lower compression duties of the PZ cases (shown in Fig. 18 and Table 6).

In addition, compared with the standard PZ-based PCC process, using AIC and AFS process configuration reduced W_{heat} by 18.9 %, and 21.1 % when using 30 wt% and 40 wt% PZ, respectively. Furthermore, the $\rm CO_2$ compressor is the second source of energy consumption in the PCC process. Through using HP and s- $\rm CO_2$ for the compressor, the compression work saving of 2.2 kJ/mol $\rm CO_2$ (21.1 % reduction) was

Table 6 Summary of energy consumption of the large-scale CO_2 capture and compression processes for a 550 MW BFPP.

	Without capture	With standa	With standard capture		With AIC and AFS		With AIC, AFS and SSE		With AIC, AFS, SSE and sCO ₂	
		30 wt% MEA	30 wt%PZ	40 wt%PZ	30 wt%PZ	40 wt%PZ	30 wt%PZ	40 wt%PZ	30 wt%PZ	40 wt%PZ
Net power output (MWe)	550.0	380.43	390.14	390.19	414.55	417.43	417.06	419.29	426.15	428.32
Net efficiency (%)	35.80	24.84	25.47	25.48	27.07	27.26	27.23	27.38	27.83	27.97
CO ₂ capture Unit										
Rich solvent pump (MWe)	N/A	0.30	0.82	0.61	0.97	0.72	1.03	0.75	1.03	0.75
Lean solvent pump (MWe)	N/A	0.030	0.030	0.023	0.011	0.008	0.011	0.008	0.011	0.008
Reboiler (MWth)	N/A	118.53	121.23	121.34	97.22	95.41	95.03	94.24	95.03	94.25
CO ₂ compression Unit										
Compressors (MWe)	N/A	42.09	32.56	32.57	32.36	32.11	32.30	32.01	25.43	25.21
S-CO ₂ pump (MWe)	N/A	N/A	N/A	N/A	N/A	N/A	N/A	N/A	3.05	3.03
S-CO ₂ turbine (MWe)	N/A	N/A	N/A	N/A	N/A	N/A	N/A	N/A	5.13	5.09
Auxiliary										
Pumps for cooling water	N/A	8.61	5.22	5.27	4.89	4.33	4.57	3.70	4.42	3.53
(MWe)										
Total power consumption (MWe)		169.57	159.86	159.81	135.45	132.57	132.94	130.71	123.85	121.68
Efficiency penalty (%)		10.96	10.33	10.32	8.73	8.54	8.57	8.42	7.97	7.83
Energy penalty (%)		30.83	29.07	29.06	24.63	24.10	24.17	23.76	22.52	22.12

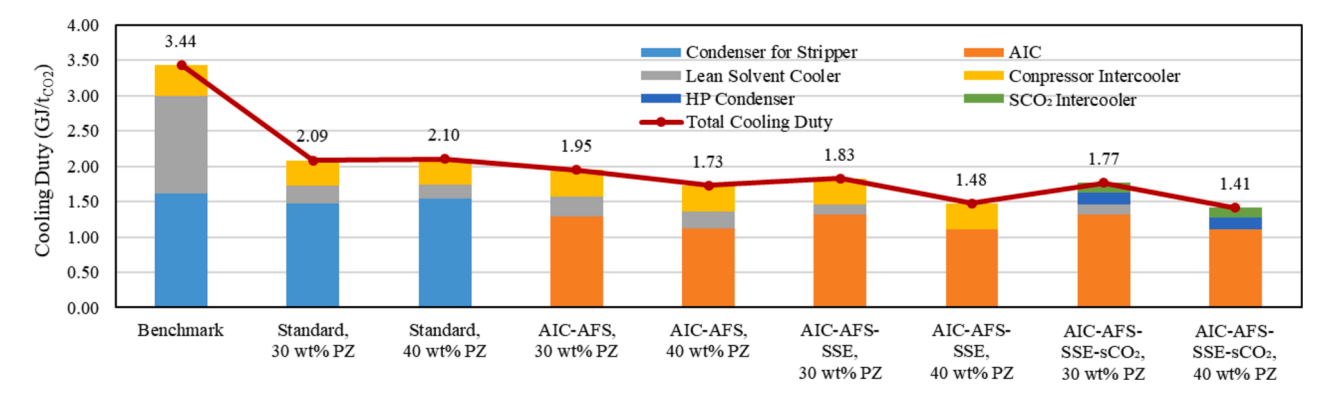


Fig. 19. Distribution of the cooling duty of different configurations.

achieved more than using the standard multi-stage compressor.

Among the eight cases, the lowest total equivalent work was obtained in the case with AIC, AFS, and SSE for the PCC process and s-CO $_2$ for the CO $_2$ compression units using 40 wt% PZ as the solvent. It reduced the total equivalent work by 10.3 kJ/mol $_{\rm CO2}$ (21.3 % saving) compared with the benchmark case.

The cooling energy demand also benefits from the application of the modified configuration. After applying the AFS configuration, the condenser is removed and replaced by the cold-rich bypass to cool down the stripper overhead vapour. As shown in Fig. 19, this can effectively reduce the cooling duty by approximately 1.5 GJ/t_{CO2} (71 % reduction). In addition, although the addition of AIC would increase the cooling duty, the total cooling duty of the AIC-AFS process still shows a reduction of 6.6 % and 17.6 % for the 30 wt% PZ and 40 wt% PZ cases, respectively. Moreover, compared with the standard MSCC, using the improved CO₂ compression configuration can also lower the cooling duty of the compression units by 16.2 % (shown in Fig. 19). This is achieved by recovering the intercooling heat through the s-CO₂ cycle.

Additionally, the energy penalty on the power plant caused by each component of the PCC process was studied. The solvent regeneration power of the reboiler is provided by the steam extracted from a 550 MW supercritical BFPP. The power of other components presented in Table 6 is provided by electricity except for the reboiler. The power loss due to the steam extraction was calculated using the required regeneration heat and a power loss factor [73]. The calculated power loss factor σ for the MEA-based benchmark case and the PZ-based cases are 0.23 and 0.25, respectively. Furthermore, the pumping power for cooling water was calculated based on Eq. (6) [73]:

$$\Delta P_{cw} = \frac{Q_{cool} \times \varphi_{cw}}{c_{p,cw} \times \Delta T_{cw}} \tag{6}$$

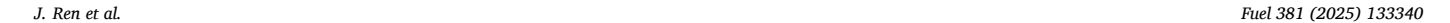
 Q_{cool} is the total cooling duty of the PCC process obtained from the simulation results. φ_{cw} is the specific auxiliary power duty obtained from Linnenberg et al. [73]. $c_{p,cw}$ is the heat capacity of the cooling water. ΔT_{cw} is the temperature increase of the cooling water and is 5 °C in this study.

Furthermore, the total effect of implementing the PCC unit on the energy performance of the 550 MW SC BFPP was evaluated using the energy penalty and efficiency penalty as the criteria. The energy penalty was calculated as the proportion of the total energy consumption of the PCC units on the net power output of the power plant. The efficiency penalty is the difference in the power plant efficiency with and without capture. The efficiency was calculated using the fuel rate of 87 kg/s and the lower heating value (LHV) of 17593 kJ/kg.

As shown in Table 6, for a 550 MW SC BFPP, utilizing the amine-based PCC process will cause an energy penalty of 22–31 %, corresponding to the efficiency penalty of 7–11 %. The process configuration with SSE and s-CO₂ using 40 wt% PZ showed the minimum total energy consumption of 121.68 MWe. This corresponds to the minimum energy penalty and efficiency penalty of 22.12 % and 7.83 %, respectively.

7. Economic analysis

The economic performance of the amine-based carbon capture and CO₂ compression processes was evaluated in APEA. APEA is considered an accurate cost-analysis tool through estimating costs from the bottom



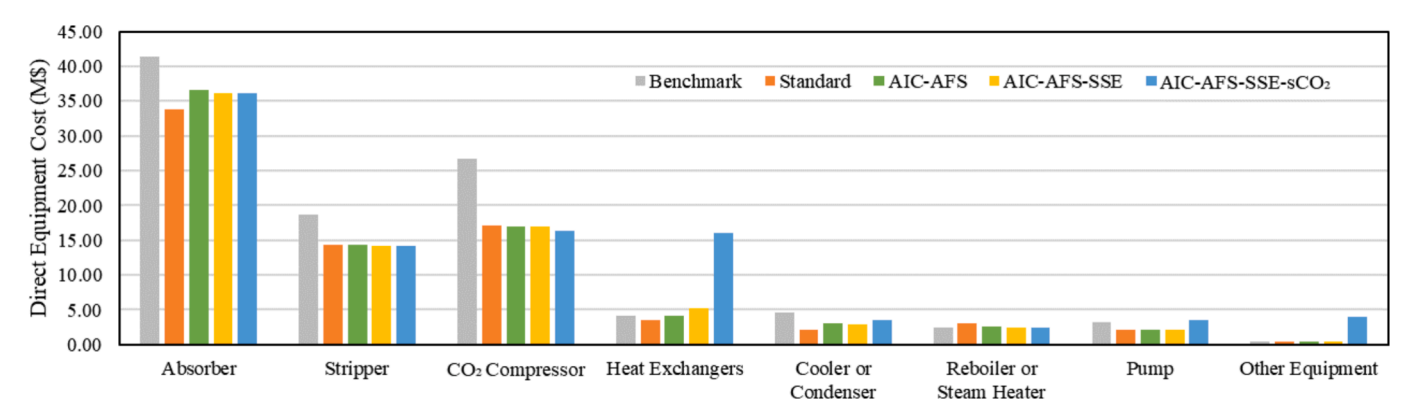


Fig. 20. Breakdown of the direct cost for different configurations using 40 wt% PZ.

Table 7Energy price for process utilities published in June 2023.

Utility type	Energy price
Electricity price (\$US/kWh) ^a	0.168
Cooling water (\$US/m ³) ^b	0.0521
Make-up water cost (\$US/m ³) ^c	1.52
Make-up MEA cost (\$US/ton) ^d	1500
Make-up PZ cost (\$US/ton) ^d	8000

- ^a price obtained from bls.gov.
- b prices obtained from intratec.us.
- ^c prices obtained from intratec.us.
- d prices obtained from alibaba.com.

up. It provides the economic evaluation through Aspen Icarus technology, which can estimate the equipment costs based on the parameters of the designed model. The total cost includes the CAPEX and the OPEX.

The total direct cost was calculated as the sum of the direct costs of each component obtained from the results of APEA. As shown in Fig. 20, among the distribution of the total direct cost, the absorber takes the largest proportion of 38–45 % followed by the compressors (16–26 %) and the stripper (15–18 %). Compared with using 30 wt% PZ solvent, using 40 wt% PZ can effectively reduce the column size when applying the same process configuration. This is due to the higher capacity of 40 wt% PZ solvent, resulting in a lower circulation solvent flow rate. Moreover, the implementation of the pump-around AIC increased the absorber cost by 5–8 %, because of the addition of some equipment such as pump and heat exchanger. Furthermore, after applying AFS, the condenser and reboiler were removed. Instead, the bypass heat exchangers and the steam heater were applied. This caused the savings of the equipment cost by 0.2 and 0.4 M\$ for the 30 wt% and 40 wt% PZ cases, respectively.

For the standard compressors, the higher cost of the MEA-based case is due to the different stripper pressures of the MEA-based (1.9 bar) and PZ-based (4.1 bar) cases. PZ can work under high pressure due to its

better resistance to thermal degradation. Additionally, using HP and s-CO $_2$ for the compressor resulted in the equipment cost rising by 13 and 16 M\$ for the processes using 30 wt% and 40 wt% PZ, respectively. The main contributor to this cost rise is the higher investment in the heat exchangers (shown in Fig. 20). In the s-CO $_2$ cycle, more heat exchangers are needed to recover the intercooling heat between the compressors and to remove heat for CO $_2$ liquefaction. However, the effect of applying the s-CO $_2$ cycle for CO $_2$ compression units on the economic performance of the whole process should be considered together with its impact on the variable O&M costs.

The CAPEX consists of the direct costs and the indirect costs. The direct costs include the cost of purchasing equipment and installed materials. The indirect costs are made up of construction expenses, engineering and contractor, legal expenses, and contingency [74]. The total CAPEX was calculated using the approach of breakdown presented by Otitoju et al. [35]. The total CAPEX is converted to the annualized capital cost (ACC) using Eq. (7):

$$ACC = CAPEX \times \frac{i(1+i)^n}{(1+i)^n - 1}$$

$$\tag{7}$$

where the interest rate i is assumed to be 10 % and the lifetime n is assumed to be 20 years.

The OPEX is divided into fixed and variable O&M costs. The fixed O&M is set as 5 % of the total capital costs. The variable O&M is evaluated as the total utility expense, which is calculated using the utility consumptions obtained from the simulation results and their energy price presented in Table 7. In this study, the $\rm CO_2$ capture cost (CCC) for capturing one tonne of $\rm CO_2$, is used as the main indicator to evaluate the economic performance. It was calculated as the total annual cost divided by the annual $\rm CO_2$ production rate ($F_{\rm CO_2,OUT}$) as shown in Eq. (8):

$$CCC = \frac{TAC}{F_{CO_2,OUT}} \tag{8}$$

Where the total annual cost (TAC) (M\$/yr) is calculated as the sum of

Table 8
Summary of the economic performance of the large-scale CO₂ capture and compression processes for a 550 MW BFPP.

	With standard capture		With IC and	With IC and AFS		With IC, AFS and SSE		With IC, AFS, SSE and s-CO2	
	30 wt%MEA	30 wt%PZ	40 wt%PZ	30 wt%PZ	40 wt%PZ	30 wt%PZ	40 wt%PZ	30 wt%PZ	40 wt%PZ
Total CAPEX(M\$)	256.41	210.88	192.84	225.98	202.12	226.55	202.80	259.76	242.04
Annual capital cost (ACC) (M\$/yr)	30.12	24.77	22.65	26.54	23.74	26.61	23.82	30.51	28.43
Fixed O&M (M\$/yr)	7.69	6.33	5.79	6.78	6.06	6.80	6.08	7.79	7.26
Variable O&M (M\$/yr):									
Electricity	227.90	214.85	214.93	182.04	178.18	178.67	175.66	166.45	163.54
Cooling water	33.49	21.64	20.96	19.85	17.08	19.31	15.30	18.63	14.64
Water make-up	1.45	2.85	3.06	4.99	4.76	5.06	5.62	5.04	5.42
Solvent make-up	0.56	1.34	2.70	2.45	4.64	2.74	5.14	2.74	5.14
Total annual cost (M\$/yr)	301.21	271.78	270.08	242.66	234.46	239.18	231.63	231.17	224.43
CO ₂ capture cost (\$/t _{CO2})	77.16	69.65	69.18	62.17	60.09	61.31	59.37	59.25	57.52

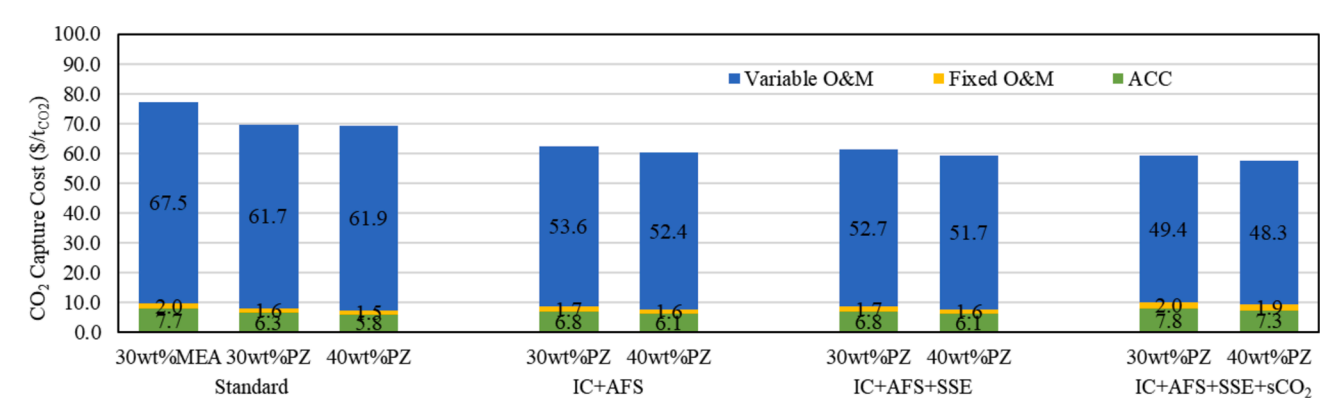


Fig. 21. Breakdown of CO₂ capture cost for a 550 MW SC BFPP.

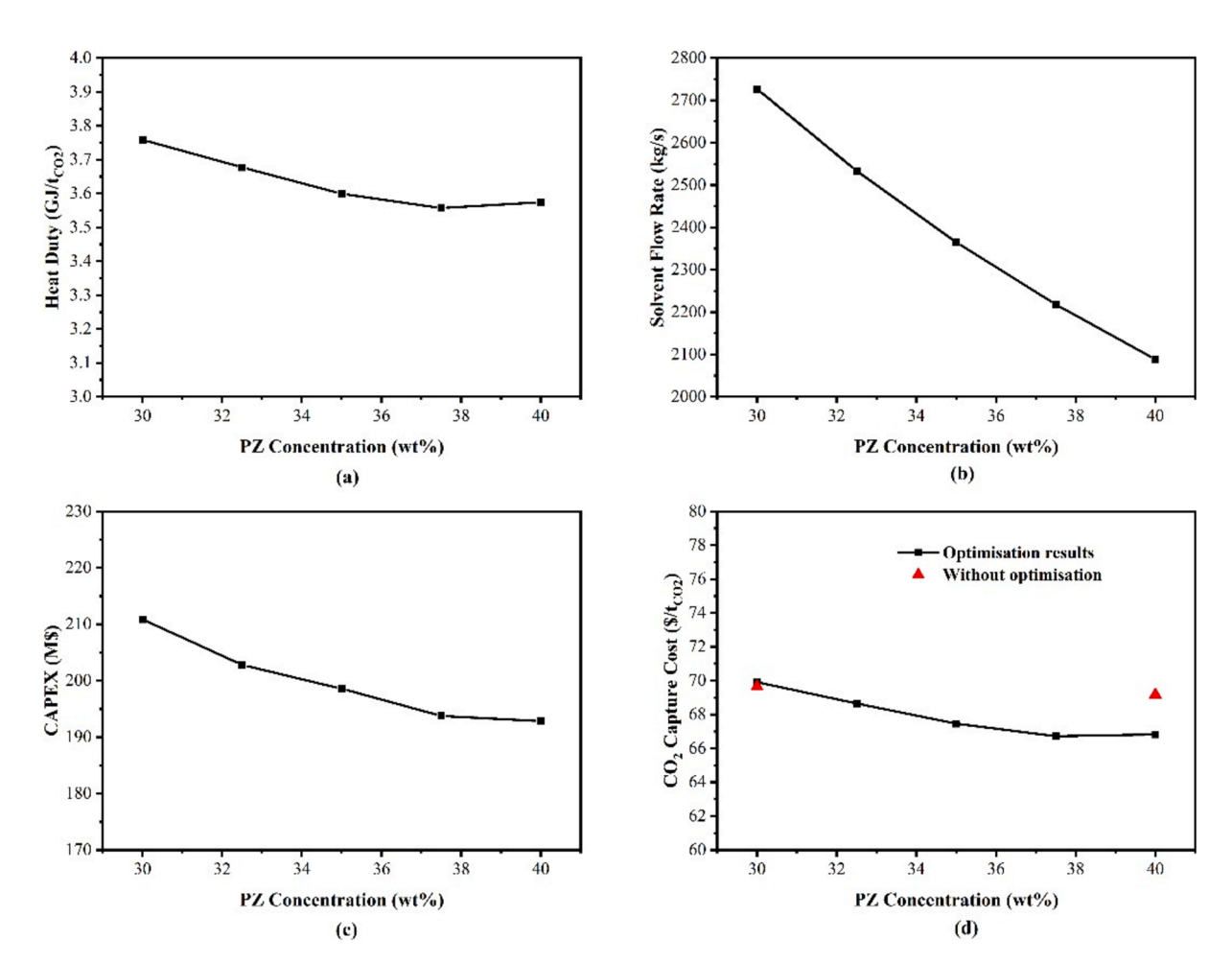


Fig. 22. Optimisation results of CCC at various PZ concentrations (standard PCC).

the ACC, fixed O&M and variable O&M.

The economic performance of different configurations is summarized in Table 8. Moreover, the breakdown of the $\rm CO_2$ capture cost is presented in Fig. 21. From the results, the higher complexity of the process configuration would lead to higher equipment costs and higher ACC. In addition, the main expense comes from the O&M costs, especially the variable O&M cost, accounting for over 80 % of the total cost. What's more, the electricity expense dominates the variable cost, followed by the cooling water expense. After analysing the economic performance of different configurations, using IC and AFS for the PCC process can reduce the $\rm CO_2$ capture cost by 12.6 % and 15.1 % for the 30 wt% and 40 wt% cases, respectively. As shown in Fig. 21, this amount of cost

saving is mainly achieved through the decline of variable O&M costs especially the electricity expense without a significant increase in the CAPEX. Moreover, the process using SSE configuration showed a slight reduction of $\rm CO_2$ capture through energy saving. For the $\rm CO_2$ compression units using HP-sCO₂, despite the increase of CAPEX by 15 %, it still showed approximately 3 % savings on the $\rm CO_2$ capture cost. This is also achieved by its lower energy penalty and lower electricity consumption.

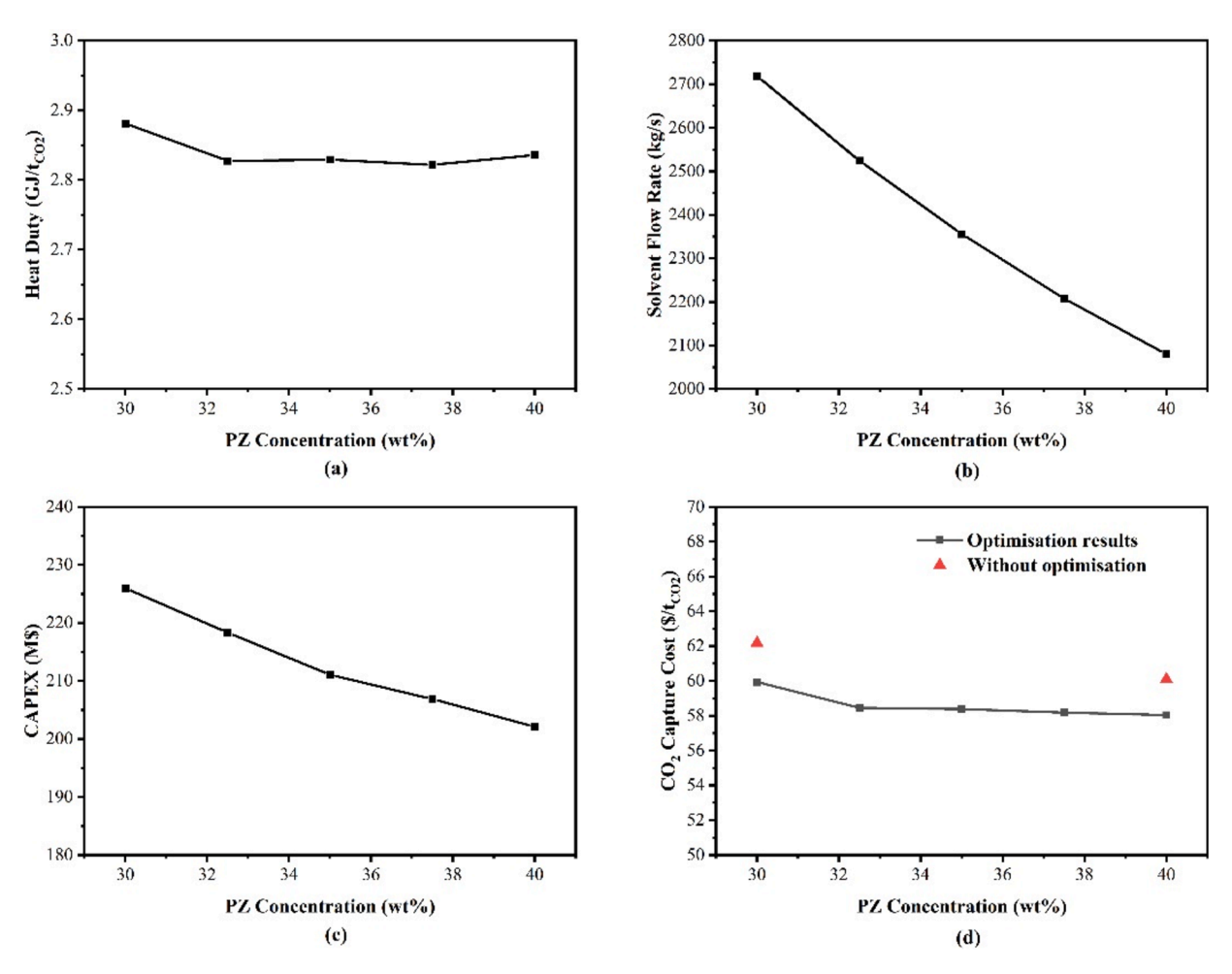


Fig. 23. Optimisation results of CCC at various PZ concentrations (AIC-AFS configuration).

8. Optimisation of PZ-based PCC process

8.1. Optimisation of PZ concentration for the solvent-based PCC process

Solvent concentration is a crucial parameter that would affect the CO_2 solubility and the regeneration energy consumption of the solvent [75]. To investigate the optimal PZ concentration with the best economic performance, the process optimisation was carried out using Aspen Plus® V11. The built-in optimisation algorithm of Aspen Plus is based on the sequential quadratic programming (SQP) method.

In this work, to obtain the best economic performance, the objective function of the optimisation is set to minimize the CCC (\$/t_{CO2}). The CCC was calculated using Eq. (19). The optimisation constraints used include the CO $_2$ capture level being set to 90 % and the PZ concentration being varied from 30 to 40 wt%. The decision variables are the heat duty for solvent regeneration and the solvent flow rate.

The results of the process optimisation for the PCC process with standard design are presented in Fig. 22. It is shown in Fig. 22 (b) that the PZ solvent with higher concentration has higher CO_2 solubility and lower solvent flow rate. Moreover, with the constant inlet flue gas flow rate, the lower solvent flow rate would result in a lower L/G ratio and thus reduce the cross-sectional area of the column, which corresponds to the smaller column size and the lower CAPEX as shown in Fig. 22 (c). What's more, when the PZ concentration increased from 30 wt% to 40 wt%, it showed a diminishing return in the decline of the heat duty (shown in Fig. 22 (a)). The heat duty for solvent regeneration takes the largest proportion of the total energy consumption and is the main contributor to the total O&M costs. The optimisation results of the CCC

were compared with the cases without optimisation and the results were presented in Fig. 22 (d). After considering the effect of the OPEX and CAPEX, it is shown that the CCC gradually declined when the PZ concentration is between 30–37.5 wt% and does not show a significant change when the PZ concentration is varied from 37.5 to 40 wt%. Thus, the optimal PZ concentration for the standard design is 37.5 wt%. Furthermore, the cost is reduced by 2.3 \$/tcO2 for the standard design using 40 wt% through this optimisation. No significant cost saving was found for the standard design using 30 wt% PZ.

Fig. 23 presented the optimisation results for the AFS design. From the results, similar trends to the standard configuration were observed. As shown in Fig. 23 (d), with the PZ concentration increasing from 30 to 32.5 wt%, the CCC reduced by 1.5 $t_{\rm CO2}$. Only a minor decline of the CCC was seen when the PZ concentration varied from 32.5 to 40 wt%. Hence, the suggested PZ concentration for the AIC-AFS configuration is 32.5 wt%. In addition, through this optimisation, the cost savings of 2.2 and 2.0 $t_{\rm CO2}$ for the 30 wt% and 40 wt% PZ cases using AFS were achieved, respectively.

8.2. Optimisation of stripper pressure for the PZ-based PCC process with AIC and AFS

With better thermal degradation resistance than MEA, PZ can operate under higher overhead stripper pressure and temperature. In the pilot plant test of NCCC reported by Gao et al. [30], the stripper pressure of 5.5–7.35 bar was applied for AFS configuration using PZ solvent. Therefore, this optimisation work is carried out to investigate the energy and economic performance of the PZ-based PCC process using AIC-AFS

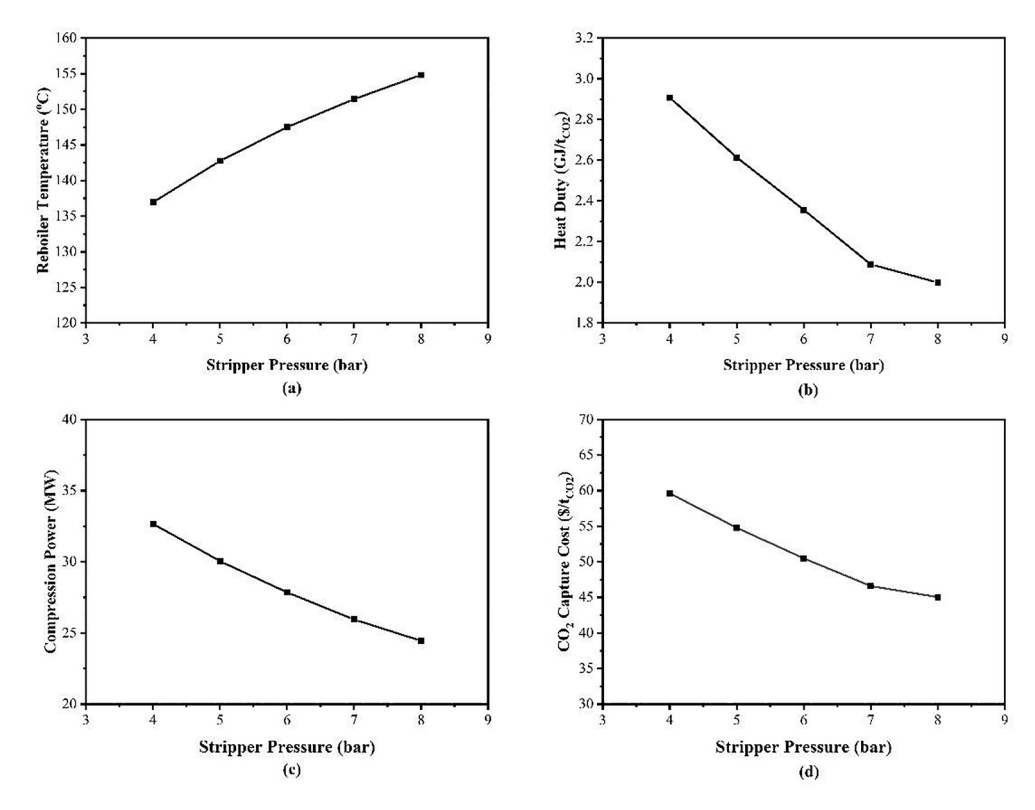


Fig. 24. Optimisation results of CO₂ capture cost at various stripper pressures for PCC process with AIC-AFS.

under high stripper pressure. The PZ concentration of 32.5 wt% was used based on the results of Section 8.1.

With the increasing stripper pressure from 4 bar to 8 bar, the stripper sump temperature was increased from 137 to 155 °C (Fig. 24 (a)), while the regeneration heat duty (Fig. 24 (b)) was reduced from 2.9 to 2.0 GJ/ $t_{\rm CO2}$. The high stripper pressure can decrease the heat duty because it can suppress the water vapour generation and hence reduce the latent heat penalty. Another advantage of applying high stripper pressure is lowering the energy required at the compression stage as shown in Fig. 24 (c). However, at the same time, to achieve the higher stripper pressure, a higher pumping power will be needed. Therefore, considering the total operating cost and capital costs, the CO₂ capture cost was calculated shown in Fig. 24 (d). It is shown that increasing stripper pressure from 4 to 8 bar can reduce the CO₂ capture cost by 14.6 \$/ $t_{\rm CO2}$. Nevertheless, Rochelle et al. [76] suggested the steam temperature up to 150 °C, or it will require a higher wall thickness for the column. Thus, the stripper pressure of 7 bar would be suggested.

9. Conclusions

In this study, the model of the PCC process using MEA and PZ as the solvent was developed and validated at a pilot scale. These models were scaled up to capture CO_2 from the flue gas of a 550 MW SC BFPP. Following this, three configurations of the PCC process and two configurations of the CO_2 compression process were simulated at a large scale in Aspen Plus®. A sensitivity analysis was carried out to investigate the effect of different parameters on the energy performance of the different configurations of the CO_2 capture and compression processes. Through the sensitivity analysis, the optimal conditions for each configuration with different concentrations of PZ (30 wt% and 40 wt%) were obtained.

Energy and cost are considered as the two main indexes for improving the performance of the PCC process. Energy analysis was conducted to evaluate the energy consumption of the different configurations of the CO_2 capture and compression processes. The results show

that the reboiler duty of the standard PCC process was reduced from 3.79 $\rm GJ/t_{CO2}$ with 30 wt% MEA to 3.58 $\rm GJ/t_{CO2}$ with 40 wt% PZ. Furthermore, a minimum heat duty of 2.78 $\rm GJ/t_{CO2}$ was achieved using AIC-AFS-SSE with 40 wt% PZ solvent. By using a compressor with HPsCO₂, a minimum total equivalent work of 37.91 $\rm kJ/mol_{CO2}$ was obtained. This corresponded to the lowest energy penalty and efficiency penalty of 22.12 % and 7.83 %, respectively.

The economic performance of eight cases was evaluated through APEA. From the results, the process configuration using AIC-AFS-SSE-sCO₂ with 40 wt% PZ showed the minimum CO₂ capture cost of 55.70 \$/t_{CO2}, which is a decrease of 19.5 % compared with the standard 40 wt % PZ case of 69.18 \$/t_{CO2}.

The optimisation of solvent concentration was carried out to find the most economical PZ concentration. The results showed that the optimal PZ concentration for the standard and AIC-AFS configurations are 37.5 wt% and 32.5 wt%, respectively. Subsequently, using the optimum PZ concentration for AFS (32.5 wt%), the optimisation on stripper pressure was carried out and a stripper pressure of 7 bar was suggested. The heat duty of 2.09 GJ/ $t_{\rm CO2}$ and $\rm CO_2$ capture cost of 46.6 \$/t_{\rm CO2} was achieved under the suggested stripper pressure. This showed a 41.6 % energy saving and 32.4 % cost saving compared with the standard PCC process using 40 wt% PZ.

CRediT authorship contribution statement

Jiayi Ren: Writing – original draft, Validation, Software, Methodology, Formal analysis, Conceptualization. Olajide Otitoju: Writing – review & editing, Supervision, Formal analysis, Conceptualization. Hongxia Gao: Writing – review & editing, Supervision. Zhiwu Liang: Writing – review & editing, Supervision. Meihong Wang: Writing – review & editing, Supervision, Funding acquisition, Conceptualization.

Declaration of competing interest

The authors declare that they have no known competing financial

interests or personal relationships that could have appeared to influence the work reported in this paper.

Data availability

Data will be made available on request.

Acknowledgement

The authors would like to thank the financial support of the EU RISE project OPTIMAL (Grant Agreement No: 101007963).

References

- IEA. CO₂ emissions in 2022. IEA 2023. https://www.iea.org/reports/co2emissions-in-2022 (accessed March 18, 2023).
- [2] IEA. Coal-fired electricity: technology deep dive. IEA 2022. https://www.iea.org/reports/coal-fired-electricity (accessed March 16, 2023).
- [3] Kemper J. Biomass and carbon dioxide capture and storage: A review. Int J Greenh Gas Control 2015;40:401–30.
- [4] Lu X, Cao L, Wang H, Peng W, Xing J, Wang S, et al. Gasification of coal and biomass as a net carbon-negative power source for environment-friendly electricity generation in China. Proc Natl Acad Sci 2019;116:8206–13.
- [5] Oh SY, Yun S, Kim JK. Process integration and design for maximizing energy efficiency of a coal-fired power plant integrated with amine-based CO₂ capture process. Appl Energy 2018;216:311–22.
- [6] Plaza JM. Modeling of carbon dioxide absorption using aqueous monoethanolamine, piperazine and promoted potassium carbonate. USA: University of Texas at Austin; 2011. PhD Thesis.
- [7] Lin YJ, Chen E, Rochelle GT. Pilot plant test of the advanced flash stripper for CO₂ capture. Faraday Discuss 2016;192:37–58.
- [8] Canepa R, Wang M, Biliyok C, Satta A. Thermodynamic analysis of combined cycle gas turbine power plant with post-combustion CO₂ capture and exhaust gas recirculation. Proc Inst Mech Eng Part E J Process Mech Eng 2013;227:89–105.
- [9] Liu X, Chen J, Luo X, Wang M, Meng H. Study on heat integration of supercritical coal-fired power plant with post-combustion CO₂ capture process through process simulation. Fuel 2015;158:625–33.
- [10] Olaleye AK, Wang M, Kelsall G. Steady state simulation and exergy analysis of supercritical coal-fired power plant with CO₂ capture. Fuel 2015;151:57–72.
- [11] Olaleye AK, Wang M. Conventional and advanced exergy analysis of postcombustion CO₂ capture based on chemical absorption integrated with supercritical coal-fired power plant. Int J Greenh Gas Control 2017;64:246–56.
- [12] Ali U, Font-Palma C, Akram M, Agbonghae EO, Ingham DB, Pourkashanian M. Comparative potential of natural gas, coal and biomass-fired power plant with post-combustion CO₂ capture and compression. Int J Greenh Gas Control 2017;63: 184–93.
- [13] Nawaz Z, Ali U. Techno-economic evaluation of different operating scenarios for indigenous and imported coal blends and biomass co-firing on supercritical coal fired power plant performance. Energy 2020;212:118721.
- [14] Hassiba RJ, Linke P. On the simultaneous integration of heat and carbon dioxide in industrial parks. Appl Therm Eng 2017;127:81–94.
- [15] Muhammad HA, Roh C, Cho J, Rehman Z, Sultan H, Baik YJ, et al. A comprehensive thermodynamic performance assessment of CO₂ liquefaction and pressurization system using a heat pump for carbon capture and storage (CCS) process. Energy Convers Manag 2020;206.
- [16] Abu-Zahra MRM, Schneiders LHJ, Niederer JPM, Feron PHM, Versteeg GF. CO₂ capture from power plants. Part I. A parametric study of the technical performance based on monoethanolamine. Int J Greenh Gas. Control 2007;1:37–46.
- [17] Abu-Zahra MRM, Niederer JPM, Feron PHM, Versteeg GF. CO₂ capture from power plants. Part II. A parametric study of the economical performance based on monoethanolamine. Int J Greenh Gas. Control 2007;1:135–42.
- [18] Amrollahi Z, Ystad PAM, Ertesvåg IS, Bolland O. Optimized process configurations of post-combustion CO₂ capture for natural-gas-fired power plant - Power plant efficiency analysis. Int J Greenh Gas Control 2012;8:1–11.
- [19] Jiang Y, Mathias PM, Freeman CJ, Swisher JA, Zheng RF, Whyatt GA, et al. Techno-economic comparison of various process configurations for postcombustion carbon capture using a single-component water-lean solvent. Int J Greenh Gas Control 2021;106:103279.
- [20] Le Moullec Y, Neveux T, Al Azki A, Chikukwa A, Hoff KA. Process modifications for solvent-based post-combustion CO₂ capture. Int J Greenh Gas Control 2014;31: 96–112.
- [21] Sultan H, H. Bhatti U, Soo Cho J, Youl Park S, Hyun Baek I, Nam S. Minimization of Energy Consumption for Amine Based CO₂ Capture Process by Process Modification. J Energy Eng 2019;28:13–8.
- [22] Muhammad HA, Sultan H, Lee B, Imran M, Baek IH, Baik YJ, et al. Energy minimization of carbon capture and storage by means of a novel process configuration. Energy Convers Manag 2020;215:112871.
- [23] Le Moullec Y, Kanniche M. Optimization of MEA based post combustion CO₂ capture process: Flowsheeting and energetic integration. Energy Procedia 2011;4: 1303–9.

[24] Zhang S, Shen Y, Zheng C, Xu Q, Sun Y, Huang M, et al. Recent advances, challenges, and perspectives on carbon capture. Front Environ Sci Eng 2024;18: 1–30.

- [25] Shao P, Ye J, Shen Y, Zhang S, Zhao J. Recent advancements in carbonic anhydrase for CO₂ capture: A mini review. Gas Sci Eng 2024;123:205237.
- [26] Freeman SA, Dugas R, Van Wagener DH, Nguyen T, Rochelle GT. Carbon dioxide capture with concentrated, aqueous piperazine. Int J Greenh Gas Control 2010;4: 119–24.
- [27] Davis JD. Thermal degradation of aqueous amines used for carbon dioxide capture. USA: University of Texas at Austin; 2009. PhD Thesis.
- [28] Rochelle GT, Chen E, Akinpelumi K, Fischer KB, Gao T, Liu C-T, et al. Pilot plant demonstration of piperazine with the advanced flash stripper. 14th Int Conf Greenh Gas Control Technol GHGT-14 2018;84:72–81.
- [29] Freeman SA, Dugas R, Van Wagener D, Nguyen T, Rochelle GT. Carbon dioxide capture with concentrated, aqueous piperazine. Energy Procedia 2009;1:1489–96.
- [30] Rabensteiner M, Kinger G, Koller M, Gronald G, Hochenauer C. Investigation of carbon dioxide capture with aqueous piperazine on a post combustion pilot plant-Part I: Energetic review of the process. Int J Greenh Gas Control 2015;39:79–90.
- [31] Ma J, Dong Z, Otitoju O, Wang M, Du W, Qian F. Heat integration, process design and techno-economic assessment of post-combustion carbon capture using piperazine for large-scale ethylene plant. Chem Eng Sci 2024;284:119531.
- [32] Nielsen PT, Li L, Rochelle GT. Piperazine degradation in pilot plants. Energy Procedia 2013;37:1912–23.
- [33] Lin YJ. Modeling advanced flash stripper for carbon dioxide capture using aqueous amines. USA: University of Texas at Austin; 2016. PhD Thesis.
- [34] Gao T, Selinger JL, Rochelle GT. Demonstration of 99% CO₂ removal from coal fl ue gas by amine scrubbing ★. Int J Greenh Gas Control 2019;83:236–44.
- [35] Otitoju O, Oko E, Wang M. Technical and economic performance assessment of post-combustion carbon capture using piperazine for large scale natural gas combined cycle power plants through process simulation. Appl Energy 2021;292: 116893.
- [36] Kurtulus K, Coskun A, Ameen S, Yilmaz C, Bolatturk A. Thermoeconomic analysis of a CO₂ compression system using waste heat into the regenerative organic Rankine cycle. Energy Convers Manag 2018;168:588–98.
- [37] Plaza JM, Rochelle GT. Modeling pilot plant results for CO₂ capture by aqueous piperazine. Energy Procedia 2011;4:1593–600.
- [38] Gaspar J, Fosbøl PL. Simulation and multivariable optimization of post-combustion capture using piperazine. Int J Greenh Gas Control 2016;49:227–38.
- [39] Pérez-Calvo JF, Mazzotti M. Techno-economic assessment of post-combustion CO₂ capture using aqueous piperazine at different flue gas compositions and flowrates via a general optimization methodology. Int J Greenh Gas Control 2022;114: 103587.
- [40] Dugas RE. Carbon dioxide absorption, desorption, and diffusion in aqueous piperazine and monoethanolamine. PhD Thesis. Dr Thesis Tech Univ Texas Austin 2009;282.
- [41] Wang M, Lawal A, Stephenson P, Sidders J, Ramshaw C. Post-combustion CO₂ capture with chemical absorption: A state-of-the-art review. Chem Eng Res Des 2011;89:1609–24.
- [42] Soave G. Equilibrium constants from a modified Redlich-Kwong equation of state. Chem Eng Sci 1972;27:1197–203.
- [43] Posey ML, Rochelle GT. A thermodynamic model of methyldiethanolamine-CO₂-H₂S-water. Ind Eng Chem Res 1997;36:3944–53.
- [44] Austgen DM, Rochelle GT, Peng X, Chen CC. Model of vapor-liquid equilibria for aqueous acid gas-alkanolamine systems using the electrolyte-NRTL equation. Ind Eng Chem Res 1989;28:1060–73.
- [45] Hetzer HB, Bates RG, Robinson RA. Dissociation constant of pyrrolidinium ion and related thermodynamic quantities from 0 to 50°. J Phys Chem 1963;67:1124–7.
- [46] Ermatchkov V, Pérez-Salado Kamps Á, Maurer G. Chemical equilibrium constants for the formation of carbamates in (carbon dioxide + piperazine + water) from 1H-NMR-spectroscopy. J Chem Thermodyn 2003;35:1277–89.
- [47] Pinsent BRW, Pearson L, Roughton FJW. The kinetics of combination of carbon dioxide with hydroxide ions. Trans Faraday Soc 1956:1512–20.
- [48] Aspentech. Rate-Based model of the ${\rm CO_2}$ capture process by MEA using Aspen Plus 11 2010:1–25.
- [49] Hikita H, Asai S, Ishikawa H, Honda M. The kinetics of reactions of carbon dioxide with monoethanolamine, and triethanolamine by a rapid mixing method diethanolamine. Chem Eng J 1977;13:7–12.
- [50] Bishnoi S, Rochelle GT. Absorption of carbon dioxide into aqueous piperazine: Reaction kinetics, mass transfer and solubility. Chem Eng Sci 2000;55:5531–43.
- [51] Bishnoi S, Rochelle GT. Absorption of carbon dioxide in aqueous piperazine/ methyldiethanolamine. AIChE J 2002;48:2788–99.
- [52] Aspentech. Rate-Based model of the ${\rm CO_2}$ capture process by mixed PZ and MDEA using Aspen Plus 11 2010.
- [53] Rackett HG. Equation of state for saturated liquids. J Chem Eng Data 1970;15: 514-7.
- [54] Bird RB, Stewart WE, Lightfoot EN. Transport Phenomena. 2nd ed. New York: John Wiley & Sons, INC; 2001.
- [55] Horvath AL. Handbook of aqueous electrolyte solutions: Physical properties, estimation and correlation methods. Chichester: Ellis Horwood; 1985.
- [56] Wilke CR, Chang P. Correlation of diffusion coefficients in dilute solutions. AIChE J 1955;1:264–70.
- [57] Poling BE, Prausnitz JM, O'Connell JP. The properties of gases and liquids. 5th ed. New York; London: McGraw-Hill; 2001.
- [58] Bravo JL, Rocha JA, Fair JR. Mass transfer in gauze packings. Hydrocarb Process 1985;64:91–5.
- [59] Packed SRF. Tower Design and Apllication. 2nd Editio. Gulf Publishing; 1987.

- [60] Chilton TH, Colburn AP. Mass transfer (absorption) coefficients: prediction from data on heat transfer and fluid friction. Ind Eng Chem 1934;26:1183–7.
- [61] Bravo JL, Patwardhan AA, Edgar TF. Influence of effective interfacial areas in the operation and control of packed distillation columns. Ind Eng Chem Res 1992;31: 604 9
- [62] Notz R, Mangalapally HP, Hasse H. Post-combustion CO₂ capture by reactive absorption: Pilot plant description and results of systematic studies with MEA. Int J Greenh Gas Control 2012;6:84–112.
- [63] Van Wagener DH. Stripper Modeling for CO₂ Removal Using Monoethanolamine and Piperazine Solvents. USA: University of Texas at Austin; 2011. PhD Thesis.
- [64] Notz R, Tönnies I, Mangalapally HP, Hoch S, Hasse H. A short-cut method for assessing absorbents for post-combustion carbon dioxide capture. Int J Greenh Gas Control 2011;5:413–21.
- [65] Netl. Greenhouse Gas Reductions in the Power Industry Using Domestic Coal and Biomass Volume 2: Pulverized Coal Plants. Natl Energy Technol Lab 2012:19–457.
- [66] Agbonghae EO, Hughes KJ, Ingham DB, Ma L, Pourkashanian M. Optimal process design of commercial-scale amine-based CO₂ capture plants. Ind Eng Chem Res 2014;53:14815–29.
- [67] Sinnott RK. Chemical engineering design. 4th ed. Oxford: Elsevier Butterworth-Heinemann; 2005.
- [68] Canepa R, Wang M. Techno-economic analysis of a CO₂ capture plant integrated with a commercial scale combined cycle gas turbine (CCGT) power plant. Appl Therm Eng 2015;74:10–9.

- [69] Gao T, Rochelle GT. CO₂ absorption from gas turbine flue gas by aqueous piperazine with intercooling. Ind Eng Chem Res 2020;59:7174–81.
- [70] Alabdulkarem A, Hwang Y, Radermacher R. Development of CO₂ liquefaction cycles for CO₂ sequestration. Appl Therm Eng 2012;33–34:144–56.
- [71] Adu E, Zhang YD, Liu D, Tontiwachwuthikul P. Parametric process design and economic analysis of post-combustion CO₂ capture and compression for coal- And natural gas-fired power plants. Energies 2020;13:1–27.
- [72] Lin YJ, Rochelle GT. Optimization of advanced flash stripper for CO₂ capture using piperazine. Energy Procedia 2014;63:1504–13.
- [73] Linnenberg S, Liebenthal U, Oexmann J, Kather A. Derivation of power loss factors to evaluate the impact of post-combustion CO₂ capture processes on steam power plant performance. Energy Procedia 2011;4:1385–94.
- [74] Chauvy R, Verdonck D, Dubois L, Thomas D, De Weireld G. Techno-economic feasibility and sustainability of an integrated carbon capture and conversion process to synthetic natural gas. J CO₂ Util 2021;47:101488.
- [75] Luo X. Process modelling, simulation and optimisation of natural gas combined cycle power plant integrated with carbon capture, compression and transport. UK: University of Hull; 2016. PhD Thesis.
- [76] Rochelle GT, Wu Y, Chen E, Akinpelumi K, Fischer KB, Gao T, et al. Pilot plant demonstration of piperazine with the advanced flash stripper. Int J Greenh Gas Control 2019;84:72–81.